THESIS

CHARACTERISTICS OF HAILSTORMS AND ENSO-INDUCED EXTREME STORM VARIABILITY IN SUBTROPICAL SOUTH AMERICA

Submitted by

Zachary S. Bruick

Department of Atmospheric Science

In partial fulfillment of the requirements

For the Degree of Master of Science

Colorado State University

Fort Collins, Colorado

Spring 2019

Master's Committee:

Advisor: Kristen L. Rasmussen

Russ S. Schumacher
V. Chandrasekar

ABSTRACT

CHARACTERISTICS OF HAILSTORMS AND ENSO-INDUCED EXTREME STORM VARIABILITY IN SUBTROPICAL SOUTH AMERICA

Convection in subtropical South America is known to be among the strongest anywhere in the world. Severe weather produced from these storms, including hail, strong winds, tornadoes, and flash flooding, causes significant damages to property and agriculture within the region. These insights are only due to the novel observations produced by the Tropical Rainfall Measuring Mission (TRMM) satellite since there are the limited ground-based observations within this region. Convection is unique in subtropical South America because of the synoptic and orographic processes that support the initiation and maintenance of convection here. Warm and moist air is brought into the region by the South American low-level jet from the Amazon. When the low-level jet intersects the Andean foothills and Sierras de Córdoba, this unstable air is lifted along the orography. At the same time, westerly flow subsides in the lee of the Andes, which provides a capping inversion over the region. When the orographic lift is able to erode the subsidence inversion, convective initiation occurs and strong thunderstorms develop. As a result, convection is most frequent near high terrain. Additionally, convection in this region often remains stationary for many hours by back-building over the high terrain, as the low-level jet continues to orographically lift unstable air over the mountains. This thesis expands the TRMM-based findings on convection in this region in two separate studies: (1) Examination of the El Nino-Southern Oscillation (ENSO)-induced convective variability and (2) Characteristics and environmental conditions supporting hailstorms. The first study uses 16 years of TRMM and reanalysis data to identify how El Nino and La Nina affect storm occurrence and characteristics in this region. While the frequency of storms does not vary greatly between ENSO phases, El Nino conditions tend to promote deeper storms with stronger convection, with more robust synoptic environments supporting convective initiation and maintenance. The second study focuses on the characteristics of the powerful hailstorms that frequent subtropical South America. Using TRMM precipitation radar and microwave imager data, hailstorms are investigated based on their probability of containing hail. Results from this study show that hailstorms have an extended diurnal cycle, often occurring in the overnight hours relative to other locations around the world. High-probability hailstorms tend to be taller and larger than storms that contain low probabilities of hail. They also tend to be supported by strong synoptic forcing, including enhanced lower- and upper-level jet streams, an anomalously warm and moist surface, and increased instability. These conditions can be forecast days in advance, which will help promote readiness and preparation for these damaging storms. Overall, these two studies further the knowledge of convection in subtropical South America, providing new information for short- and long-term forecasts of convection and context to the results of the recent RELAMPAGO field campaign.

ACKNOWLEDGEMENTS

I would like to thank Kristen Rasmussen for giving me the opportunity to work in her research group. Without her support, guidance, and mentorship over the last two years, none of this would have been possible. I could not ask for a better advisor. Many thanks to my committee members, Russ and Chandra, for their feedback throughout the writing of this thesis. I would also like to thank my coauthors of the two papers included within this thesis for their time and effort in these collaborations, which significantly improved the quality of my work. This research was sponsored by National Science Foundation Grants AGS-1661657 and AGS-1661768, and an American Meteorological Society/NASA Earth Science Graduate Fellowship. Finally, I need to thank Samantha Bruick for her unending support from my first day in this program - without her, I would be lost.

TABLE OF CONTENTS

LIST OF TABLES

LIST OF FIGURES

Chapter 1

Introduction

Severe convection causes major disruptions to life, property, and economic stability, no matter where it occurs in the world. In subtropical South America, where a majority of economic activity is concentrated in the agricultural sector, severe weather can be catastrophic to economic stability and societal well-being. While severe thunderstorms have been documented in this region since the mid-20th century, it wasn't until the advent of the space-borne radar, namely with the launch of the Tropical Rainfall Measuring Mission (TRMM) satellite in 1997, that research on these powerful storms began. Since then, convection on global and regional scales has been reexamined over the past two decades. With this new source of data, subtropical South America was identified for the first time as one of the locations with the strongest convection anywhere in the world (Zipser et al. 2006). Furthermore, these storms have been found to frequently be severe, with hail, flash flooding, and occasional tornadoes (Rasmussen et al. 2014).

While thunderstorms in subtropical South America have been anecdotally documented since the 1960s (Grandoso and Iribarne 1963), the TRMM satellite's Precipitation Radar (PR) provided the first regular three-dimensional observations of convection in this region. In-depth studies of subtropical South American convection using TRMM PR data found that storms in this region are uniquely forced by the complex terrain of the Andes Mountains and other smaller mountain ranges, and supported by moisture from the "green ocean" of the Amazon rainforest (Rasmussen and Houze 2011, 2016; Mulholland et al. 2018). Their formation is supported by the South American low-level jet's (SALLJ) interaction with the Andes and Sierras de Córdoba, a secondary mountain range east of the main Andes barrier, which both provide orographic forcing to overcome synoptic subsidence and its resultant convective inhibition in the lee of the Andes (Rasmussen and Houze 2011, 2016). These unique synoptic ingredients and the resulting intense, frequent, and stationary convection have spurred recent large-scale research efforts within subtropical South America, including the Remote sensing of Electrification, Lightning, And Mesoscale/microscale Processes with Adaptive Ground Observations (RELAMPAGO) field campaign[1] (1 November - 17 December 2018), which observed thunderstorms near the Sierras de Córdoba with ground-based instrumentation for the first time. In order to prepare for this campaign, this thesis presents background studies on convection in this region to better understand 1) how the El Niño-Southern Oscillation influences convection and 2) why the convection in subtropical South America produces large and frequent hail.

The variability of convection due to the El Niño-Southern Oscillation (ENSO) in subtropical South America is studied using TRMM PR observations and ERA-Interim reanalysis data from 1998-2013. The findings of this research, presented in Chapter 2, have been accepted for publication, pending revisions, in *Monthly Weather Review*[2]. Previous research has found that ENSO has a strong influence on precipitation patterns in tropical and subtropical South America. Specifically, precipitation is increased during El Niño in the La Plata basin of eastern subtropical South America and decreased in tropical regions (Liebmann and Marengo 2001; Camilloni and Barros 2003; Espinoza Villar et al. 2009; Cavalcanti et al. 2015; Shimizu et al. 2017). During La Niña, the anomalies reverse and precipitation increases over the Amazon. These anomalies are the results of anomalous Hadley and Walker circulations over tropical South America (Liebmann and Marengo 2001), as well as shifts in the South Atlantic Convergence Zone (Grimm et al. 2000; Grimm and Tedeschi 2009). However, no prior studies have focused on the variability of convection and associated storm characteristics within subtropical South America due to ENSO.

Using the aforementioned satellite and reanalysis model data, this study found that different phases of ENSO does not greatly inhibit or promote convective development in this region. Rather, the frequency and intensity of the most extreme convection was modulated by the different phases of ENSO. Storms during El Niño tend to contain more intense convection and are supported by a more favorable synoptic environment. This enhanced synoptic support comes mainly from en-

[1]https://www.eol.ucar.edu/field_projects/relampago

[2]Bruick, Z. S., K. L. Rasmussen, A. K. Rowe, and L. A. McMurdie, 2019: Characteristics of Intense Convection in Subtropical South America as Influenced by El Niño-Southern Oscillation. Mon. Weather Rev., accepted, pending revisions.

hanced jet strength and conditional instability within subtropical South America. Precipitation from these extreme storms does not vary greatly between phases of ENSO, so it is hypothesized that the precipitation anomalies previously found in eastern subtropical South America are a result of differences in the duration of storms, which could not be observed by the TRMM satellite, or by changes to the frequency or intensity of less intense convection. The findings of this study inform researchers, operational meteorologists, and other interested groups that intense storms in subtropical South America will continue to present significant hazards to this region regardless of ENSO phase.

The second study contained in this thesis focuses on the frequent severe hailstorms within subtropical South America using the same TRMM PR and ERA-Interim data, along with the TRMM Microwave Imager (TMI). The results of this work have been submitted for review to *Monthly Weather Review* as well[3]. Cecil and Blankenship (2012) found subtropical South America to be a hotspot for hail activity worldwide using AMSR-E and TMI observations to create a proxy for the probability of large hail (i.e., 1 inch or greater) within convection. Ground-based studies have found hail to be frequent from Mendoza to the central plains near Córdoba (Mezher et al. 2012), with large hail ($>$ 2 cm) causing 80% of the agricultural damages in this region (Perez and Puliafito 2006). These past studies have relied upon surface station data, which come from a sparse network and are dependent upon reports from weather observers. There is no centralized database of reports from the public, such as the database produced by the Storm Prediction Center in the U.S.[4], or a sufficient radar network to create a radar-derived hail climatology (e.g, Cintineo et al. 2012), due to the lack of S-band radars in Argentina. As a result, ground-based climatologies of hailstorms in subtropical South America are unable to capture the full distribution of these damaging storms. Therefore, this study sought to advance the work of Cecil and Blankenship (2012) and their satellite-based method. This technique is useful for the development of objective climatologies wherever there are no adequate ground-based observational networks. The study, contained in

[3]Bruick, Z. S., K. L. Rasmussen, and D. J. Cecil, 2019: Subtropical South American Hailstorm Characteristics and Environments. Mon. Wea. Rev. Submitted for review.

[4]https://www.spc.noaa.gov/exper/reports/

Chapter 3, demonstrates that hailstorms have an extended diurnal cycle as compared to hailstorms in the U.S. Hailstorms in subtropical South America can occur well after midnight, significantly extending their damage potential. With regard to storm characteristics, convective storms with high probabilities of hail are more likely to be deeper and wider than storms with low probabilities of hail. Convection within hailstorms is stronger, and these storms are also more likely to be multi-cellular in nature, which is a significant difference from hailstorms found in the U.S. Finally, hailstorms in subtropical South America are supported by robust synoptic environments that allow for the development of intense convection. These patterns can be used to better forecast the occurrence of hail hours and days in advance of any hailfall and will also improve the understanding of hailstorms in other regions of the world.

Chapter 2

Characteristics of Intense Convection in Subtropical South America as Influenced by El Niño–Southern Oscillation

El Niño–Southern Oscillation (ENSO) is known to have teleconnections to atmospheric circulations and weather patterns around the world. Previous studies have examined connections between ENSO and rainfall in tropical South America, but little work has been done connecting ENSO phases with convection in subtropical South America. The Tropical Rainfall Measuring Mission (TRMM) Precipitation Radar (PR) has provided novel observations of convection in this region, including that convection in the lee of the Andes Mountains is among the deepest and most intense in the world with frequent upscale growth into mesoscale convective systems. A 16-year dataset from the TRMM PR is used to analyze deep and wide convection in combination with ERA-Interim reanalysis storm composites. Results from the study show that deep and wide convection occurs in all phases of ENSO, with only some modest variations in frequency between ENSO phases. However, the most statistically significant differences between ENSO phases occur in the three-dimensional storm structure. Deep and wide convection during El Niño tends to be taller and contain stronger convection, while La Niña storms contain stronger stratiform echoes. The synoptic and thermodynamic conditions supporting the deeper storms during El Niño is related to increased convective available potential energy, a strengthening of the SALLJ, and a stronger upper-level jet stream, often with the equatorward-entrance region of the jet stream directly over the convective storm locations. These enhanced synoptic and thermodynamic conditions provide insight into how the structure of some of the most intense convection on Earth varies with phases of ENSO.

2.1 Introduction

Precipitating systems are a critical component of Earth's hydrologic and energy budgets by redistributing moisture and energy. Extreme precipitation events usually take the form of convective storms, which have a large socioeconomic impact through flooding, large hail, and extreme winds. Around the world, the variability of convection causes hydrological extremes such as droughts and floods that significantly affect large regions for an extended amount of time. Additionally, the occurrence of extreme events and associated severe weather impacts have been related to large-scale climate variability (Cook and Schaefer 2008; Tippett et al. 2015; Rasmussen et al. 2014; Cook et al. 2017) with one notable example of large-scale variability being the El Niño–Southern Oscillation (ENSO). ENSO is an interannual fluctuation of tropical Pacific Ocean sea surface temperatures and the surface pressure difference between Darwin and Tahiti (Trenberth 1997) that is known to affect the variability of temperature and precipitation globally on an interannual cycle through teleconnections (Wallace and Gutzler 1981; Horel and Wallace 1981; Rasmusson and Carpenter 1983; Ropelewski and Halpert 1987; Halpert and Ropelewski 1992; Dai 2001). Thus, a greater understanding of the role of ENSO on the global variability of convection and associated severe weather and flooding will help improve high-impact weather predictability.

Under neutral ENSO conditions, the Walker circulation transports warm, moist air to the western Pacific Ocean where it rises and returns aloft to the eastern Pacific where it descends and flows west once more (Bjerknes 1969). During the warm phase of ENSO, commonly referred to as El Niño, the Walker circulation weakens or breaks down, leading to the anomalous convergence of air in the central Pacific Ocean and an increase in the frequency of convection and lightning there (Chronis et al. 2008), and anomalous subsidence over tropical South America (Shimizu et al. 2017). During the cold phase of ENSO, known as La Niña, the Walker circulation strengthens, but remains in the same place as in neutral conditions, with a rising branch of the circulation over tropical South America. Additionally, the Hadley circulation, which has its rising branch near the equator and sinking branch at 30°S, is weakened during El Nino by the reduced convective activity in northern South America (Grimm and Ambrizzi 2009).

These changes in the Walker and Hadley circulations modulate global circulations by disrupting the propagation of Rossby waves generated by tropical convection (Grimm and Ambrizzi 2009). Therefore, ENSO impacts convection globally. In the United States (U.S.), increased rainfall from mesoscale convective systems (MCSs; Anderson and Arritt 2001) and increased precipitation over the southern states and Gulf of Mexico (Dai 2001; Lee et al. 2014) are correlated with El Niño, while more severe weather events in the southeast U.S. occur during La Niña (Allen et al. 2015). In southeast Asia, El Niño causes higher surface pressure over the ocean, leading to onshore flow and increased precipitation over land (Yoshida et al. 2007). Farther south in Indonesia, colder ocean waters during El Niño decrease convection, which leads to enhanced drought conditions during summer (Hendon 2003).

Recent research has examined how ENSO affects rainfall in tropical regions of South America, such as the Amazon rainforest in northern South America. Shimizu et al. (2017) showed that the Amazon and northeastern Brazil are drier during El Niño due to anomalous subsidence from disrupted Walker and Hadley circulations. This result corroborated previous studies that found that warmer tropical central Pacific Ocean temperatures during El Niño shortened the convective season in the Amazon (Liebmann and Marengo 2001) and decreased rainfall over the northeastern Amazon and southern tropical Andes mountains (Espinoza Villar et al. 2009). In subtropical South America, correlations between rainfall and ENSO have been demonstrated, especially for the La Plata basin encompassing northeast Argentina, Paraguay, and southeastern Brazil. Rainfall tends to be maximized in this area during El Niño, leading to flooding within the basin (Camilloni and Barros 2003; Cavalcanti et al. 2015). Synoptic forcing for enhanced rainfall in the La Plata basin may be provided by a stronger subtropical jet with increased cyclonic vorticity advection, as well as enhanced moisture advection from the Amazon and tropical Atlantic Ocean into the basin (Karoly 1989; Grimm et al. 2000; Grimm and Tedeschi 2009). However, an understanding of how specific characteristics of precipitation systems and convective storms in subtropical South America are influenced by ENSO is lacking given the remote location and general scarcity of ground-based observations in the region.

The Tropical Rainfall Measuring Mission (TRMM) satellite's Precipitation Radar (PR) is the only long-term observational dataset available to examine convection in subtropical South America. Using the TRMM PR, convection in this region has been found to be some of the most intense anywhere on Earth (Zipser et al. 2006; Romatschke and Houze 2010; Houze et al. 2015). Storms frequently initiate near the elevated terrain of the Andean foothills and the Sierras de Córdoba (SDC) in western and central Argentina (Fig. 2.1). Rasmussen et al. (2016) developed a con-

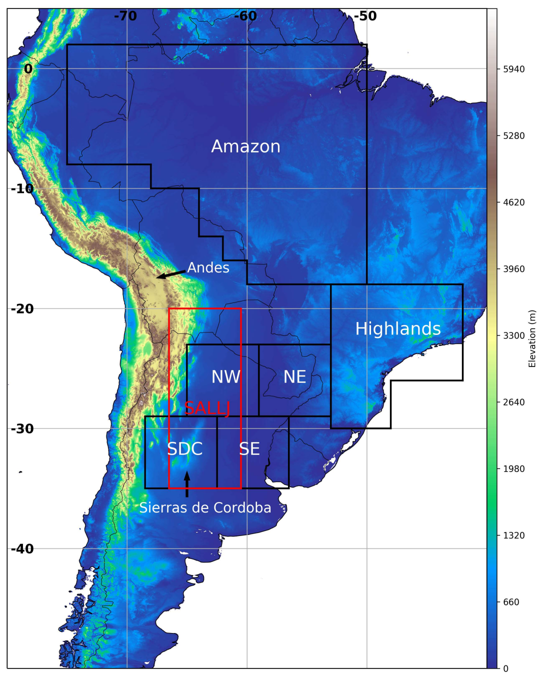

Figure 2.1: South America with topography and study sectors overlaid. The four 6° by 6° primary sectors located in northern Argentina and Paraguay and the Amazon and Highland comparison sectors are based on the climatology of Rasmussen et al. (2016). The South American Low-Level Jet (SALLJ) region is based on Rasmussen and Houze (2016).

ceptual model to show why this region is highly favored for convective initiation and subsequent upscale growth. Convergence is maximized near the SDC due to the impingement of the South American low-level jet (SALLJ) from the north and ageostrophic mid-level flow from the south on the elevated terrain. Due to the descent of upper-level air in the lee of the Andes, a mechanical capping inversion exists over the region that inhibits convective initiation. Moisture is advected into subtropical South America from the Amazon rainforest to the north via the SALLJ and from the subtropical Atlantic Ocean to the northeast, which destabilizes the near-surface atmosphere. With sufficient topographic forcing provided by the SDC and the Andean foothills, the capping inversion is broken and convective initiation occurs (Rasmussen and Houze 2016). Storms initially grow very deep and are capable of producing large hail, strong winds, and flooding rains (Rasmussen et al. 2014). As storms move east off the terrain, they tend to grow upscale into MCSs, occasionally featuring repeated development of intense convective elements along the terrain referred to as back-building due to continued moisture advection and uplift by the SALLJ (Velasco and Fritsch 1987; Rasmussen et al. 2014; Rasmussen and Houze 2011, 2016). MCSs provide approximately $15-21\%$ of annual rainfall (Durkee et al. 2009) and 44% of the warm-season rainfall (Rasmussen et al. 2016) in the La Plata basin of northeastern Argentina, Paraguay, and southern Brazil, making them important rainfall producers during the growing season.

Due to the extreme nature of convection in subtropical South America, with regards to intensity and frequency, improved understanding of how different phases of ENSO may affect the frequency, intensity, and storm characteristics of high-impact storms in this region will broadly enhance knowledge on the interactions of deep convection and complex topography in varying environments. This study examines how the frequency and characteristics of convection change with respect to El Niño and La Niña in subtropical South America. Variations in synoptic conditions between El Niño and La Niña, derived from reanalysis data, help to explain the differences in convective characteristics found in the satellite observations. Additionally, these results provide insight on important synoptic conditions leading to some of the most intense convection in the world. Storms in subtropical South America occur over important agricultural areas that support a large portion of the region's economy, thus a greater understanding of the variability of high-impact storms in the region have large socioeconomic benefits. Finally, this study will provide context as to how ENSO may impact the RELAMPAGO field campaign, which seeks to further the understanding of convective storms in Argentina through extensive field observations.

2.2 Methodology

To study the intense convection in subtropical South America concentrated near the Andes and SDC (Romatschke and Houze 2010; Rasmussen and Houze 2011; Rasmussen et al. 2016), four primary sectors, each $6°$ by $6°$, are defined over this area (Fig. 2.1). These regions contain much of subtropical South America and will be referred to as such throughout the study. The southwestern sector (SDC) is located over the SDC range. The northwest (NW) sector is located north of the SDC sector with its western edge along the lee slope of the Andes, as convection is known to initiate along the terrain in this region. The northeast (NE) and southeast (SE) sectors are located immediately to the east of the NW and SDC sectors, respectively, to capture the upscale growth of MCSs as they move east off the high terrain (Rasmussen and Houze 2011, 2016; Rasmussen et al. 2014). The Amazon and Highlands regions are included as reference areas (Rasmussen et al. 2016) to compare to previous ENSO studies in tropical South America (e.g., Grimm et al. 2000; Liebmann and Marengo 2001; Espinoza Villar et al. 2009).

To assess the phase of ENSO in any given month, the Niño 3.4 standardized temperature anomalies are used. The Niño 3.4 region extends from $5°$N to $5°$S and $120°$W to $170°$W in the central tropical Pacific Ocean. This region has been used by the National Centers for Environmental Prediction's Climate Prediction Center since 1996 to analyze the phase and magnitude of ENSO (Trenberth 1997). The standardized anomalies are calculated using the Hadley Centre sea ice and sea surface temperature data set version 1 (HadISST1; Rayner et al. 2003). An El Niño or La Niña event is determined to have occurred if the standardized temperature anomaly is above or equal to 0.5 K, or below or equal to -0.5 K, respectively, for six months or longer (Trenberth 1997). This index has been used in many studies, including the recent studies of Blamey et al. (2017), Sulca Juan et al. (2017), and Parhi et al. (2015), although they make use of other, but similar, oceanic temperature reanalysis datasets.

To analyze the characteristics of convection, a 16-year dataset (1998-2013) from TRMM is utilized. The TRMM PR had a high spatial resolution ($4-5$ km horizontal, 250 m vertical), with coverage between 36°N and 36°S (Kummerow et al. 1998, 2000). Three TRMM data products are used in this study:

- 2A23 (rain characteristics; Awaka et al. 1997), where TRMM orbital precipitation data is separated into the three categories of convective, stratiform, and other.
- 2A25 (rainfall rate and profile; Iguchi et al. 2000), which contains the TRMM orbital three-dimensional attenuation-corrected reflectivity data.
- 3B43 (rainfall climatologyj Huffman et al. 2007), which provides gridded monthly multi-satellite calibrated precipitation, output on a monthly basis.

Following the methodology of Houze et al. (2007), the TRMM PR data is processed from the original orbital data from the conical-scanning radar and is remapped by implementing a geolocation algorithm and interpolated into Cartesian coordinates. Using this data, storms containing deep and wide convective echoes are identified using a methodology established by the same study. Deep convective cores (DCCs) are three-dimensional contiguous cores with 40-dBZ echoes $\geq$ 10 km altitude, and represent vigorous convection that contains strong and tall updrafts early in the convective lifecycle. Wide convective cores (WCCs) are three-dimensional contiguous 40-dBZ echoes with maximum horizontal area coverage of $\geq$ 1000 km^2 and are representative of MCSs that have become very large horizontally and yet remain extremely intense, which allows them to be capable of producing substantial rainfall and occasional severe weather (Houze 2004). Deep and wide convective cores (DWCCs) must meet the criteria of both DCCs and WCCs and are an exclusive category so that no storms exist in more than one category. DWCCs represent vigorous convection that has begun to grow upscale with intense horizontal and vertical components. These methods have been utilized by numerous studies including Romatschke and Houze (2010), Rasmussen et al. (2014, 2016), Qie et al. (2014), Roy et al. (2014), Zuluaga and Houze (2015), and many others. While the method described above identifies convective cores using TRMM PR data, the full storm that each convective core is embedded within is analyzed in the current study to present a holistic picture of how convective systems may vary due to ENSO. Two-sided t-tests were conducted on the TRMM-derived storm characteristics to identify statistically significant differences between ENSO phases.

The TRMM PR rainfall algorithm is known to underestimate precipitation produced by deep convection over land (Iguchi et al. 2009; Rasmussen et al. 2013). Therefore, rainfall was instead estimated with the *Z-R* relationship used by Rasmussen et al. (2013), $Z = aR^b$, where Z is the radar reflectivity factor ($mm^6\ m^{-3}$) and R is the corrected rain rate ($mm\ h^{-1}$). The parameters a and b are constants based on rain type. The values used to calculate rainfall in this study were previously implemented by Romatschke and Houze (2011) and Rasmussen et al. (2013, 2016) for typical subtropical land-based rainfall, where $a = 100$ and $b = 1.7$ for convective rain, and $a = 200$ and $b = 1.49$ for stratiform rain.

To analyze the vertical structure of storms containing DCCs, DWCCs, and WCCs, Contoured Frequency by Altitude Diagrams (CFADs) are used (Yuter and Houze 1995). These plots compress three-dimensional data into a two-dimensional histogram in order to show the frequency of a specific reflectivity echo at a particular altitude. The frequency is normalized at each level by the most frequent reflectivity bin found within that level. Precipitation-type CFADs are created using the 2A23 TRMM product to distinguish between stratiform and convective rain.

Synoptic and environmental conditions are derived from ERA-Interim reanalysis (Dee et al. 2011) with all variables computed at 18 UTC on the day of storm occurrence. El Niño and La Niña climatological conditions are composited from 1980-2009 using the ERA-Interim Synoptic Monthly Means product, with months selected for each ENSO phase based on the Niño 3.4 temperature anomalies discussed above.

2.3 ENSO Climatological Rainfall and Synoptic Conditions

During El Niño, much of subtropical South America, including the four primary sectors, experiences increased rainfall on the order of $20-60$ mm more per month than climatology (Fig. 2.2a). Enhanced rainfall is maximized across northeastern Argentina and southeastern Brazil, with almost no difference between El Niño months and climatology across the Andean foothills in western Ar-

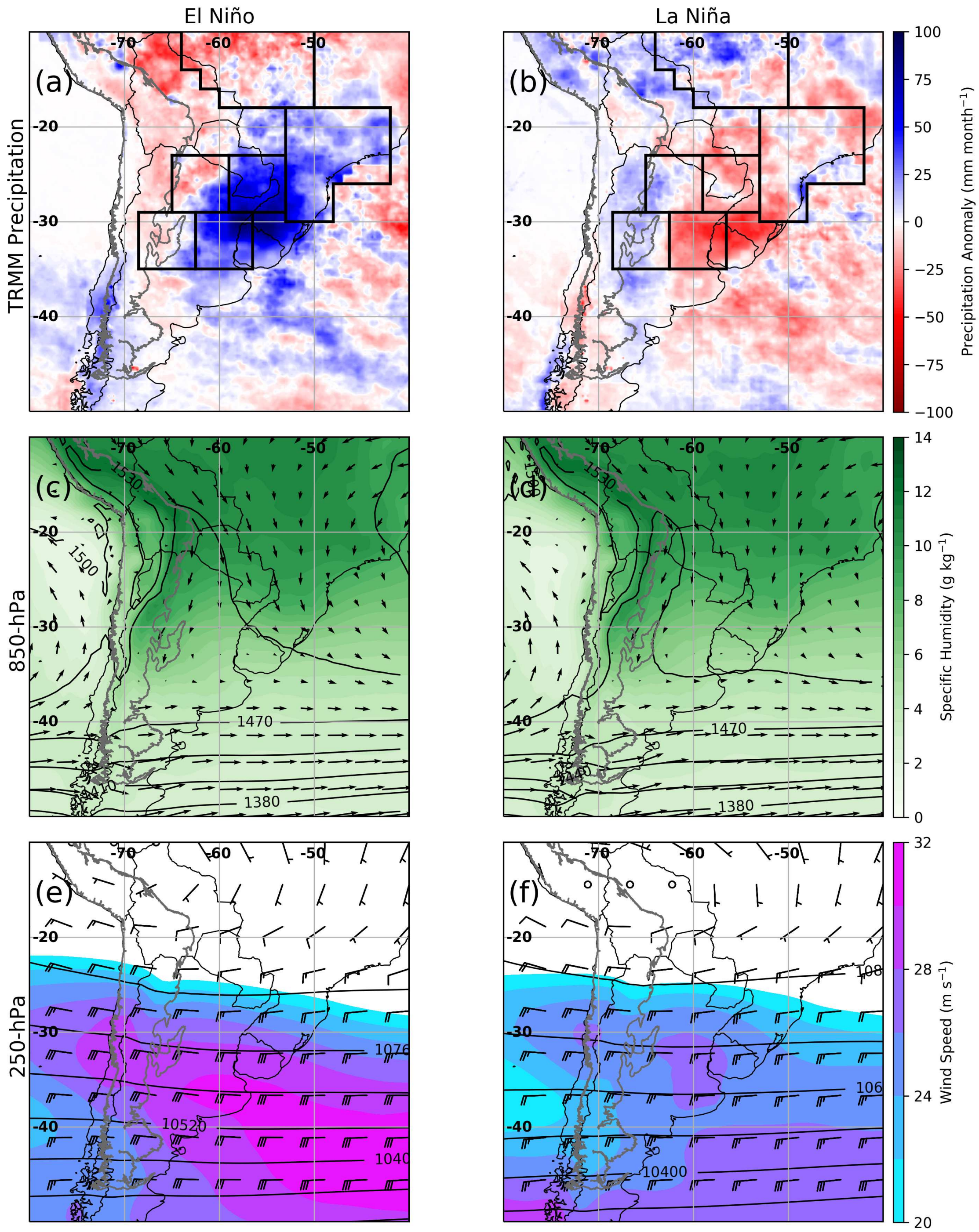

Figure 2.2: Panels a and b show the differences between El Niño and La Niña rainfall from TRMM climatology (mm/month; a, b), respectively, for September through February. The ERA-Interim 1980-2009 composite climatology is shown for El Niño and La Niña 850-hPa geopotential height (m), wind speed (m s-1), and specific humidity (g kg-1; c, d) and 250-hPa geopotential height and wind speed (e, f). The 500-m topographic isopleth is contoured in grey and the sectors outlined in Figure 2.1 are included in panels a and b for reference.

gentina. During La Niña, the pattern reverses, with diminished rainfall compared to climatology across northeastern Argentina and southeastern Brazil, including the NE and SE study regions and enhanced rainfall over the SDC and NW regions (Fig. 2.2b). Rainfall also increases during La Niña in Bolivia and western Brazil. It is important to note that rainfall correlates with ENSO seasonally in this region, as previous research has shown that the strongest correlations between El Nino and rainfall occur in the spring across northern Argentina (Gonzalez et al. 2017).

The precipitation anomaly results during El Niño are similar to findings from Ropelewski and Halpert (1987) and Souza and Ambrizzi (2002). Both studies found precipitation maxima in the northeastern Argentina, Uruguay, and southeastern Brazil during El Niño periods using surface and satellite measurements, respectively. Ropelewski and Halpert (1987) hypothesize that this precipitation anomaly is due to stronger upper-level westerly flow and increased low-level convergence. Grimm and Tedeschi (2009) found that the regional circulation over eastern Brazil tends to be cyclonic during El Niño. This circulation brings more moisture to subtropical South America, which helps to increase precipitation. The increased La Niña rainfall in Bolivia and western Brazil found in this study concurs with previous surface station results from Espinoza Villar et al. (2009) and Shimizu et al. (2017). Increased rainfall over the Amazon during La Niña is a result of increased moisture convergence due to a regional anticyclonic circulation (Grimm and Tedeschi 2009) and a strengthened Walker circulation (Shimizu et al. 2017).

Enhanced low- and upper-level jet streams and a broader lee trough during El Niño are highlights of the climatological synoptic conditions for El Niño and La Niña, using 1980-2009 ERA-Interim composites (Fig. 2.2). The 850-hPa winds are stronger near the elbow of the Andes and into Paraguay during El Niño, indicating an enhancement of the SALLJ (Fig. 2.2c). The upper-level jet is stronger during El Niño, with maximum climatological wind speeds exceeding 30 m s^{-1} over the central Andes and from east-central Argentina into the southern Atlantic Ocean (Fig. 2.2e), with the maximum difference occurring during spring (not shown). This increased upper-level jet strength over subtropical South America during El Niño was originally noted by Arkin (1982) and hypothesized to be a result of a strengthened Hadley circulation during El Niño

(Kousky et al. 1984). Additionally, a broader lee trough exists at 850 hPa during El Niño, where the 1500-m geopotential height contour extends farther east into central Argentina (Figs. 2.2c, d). This feature is also evident in the surface mean sea-level pressure field (not shown). Lee cyclogenesis has been identified as a key feature associated with convection in subtropical South America (Rasmussen and Houze 2016) and has been identified in the U.S. as being present before severe convection initiates in some cases (e.g., Karyampudi et al. 1995). Moisture within the SALLJ box outlined in Figure 2.1 is comparable between El Niño and La Niña (Table 2.1). However, moisture

Table 2.1: 850-hPa climatological conditions within the SALLJ box outlined in Figure 2.1.

	850 Specific Humidity (g kg^{-1})	850 Winds (m s^{-1})
El Niño	7.50	2.89
La Niña	7.48	2.64

advection into the study regions is slightly enhanced during El Niño (not shown) due to the stronger and broader low-level jet (Fig. 2.2c). With increased moisture advection, and stronger lower- (Table 2.1) and upper-level jets, storm environments in subtropical South America are enhanced on average during El Niño conditions relative to La Niña.

2.4 Variability of Convective Storms and their Environments during ENSO

2.4.1 Synoptic Environment Differences

Although the study period is limited to the lifetime of the TRMM satellite, a large number of convective storms were captured by the TRMM PR across four El Niños and four La Niñas (Fig. 2.3) during austral spring and summer, enabling further analysis into differences in storm characteristics and their supporting synoptic environments between ENSO phases. To assess the differences between the climatological El Niño and La Niña environments with convective envi-

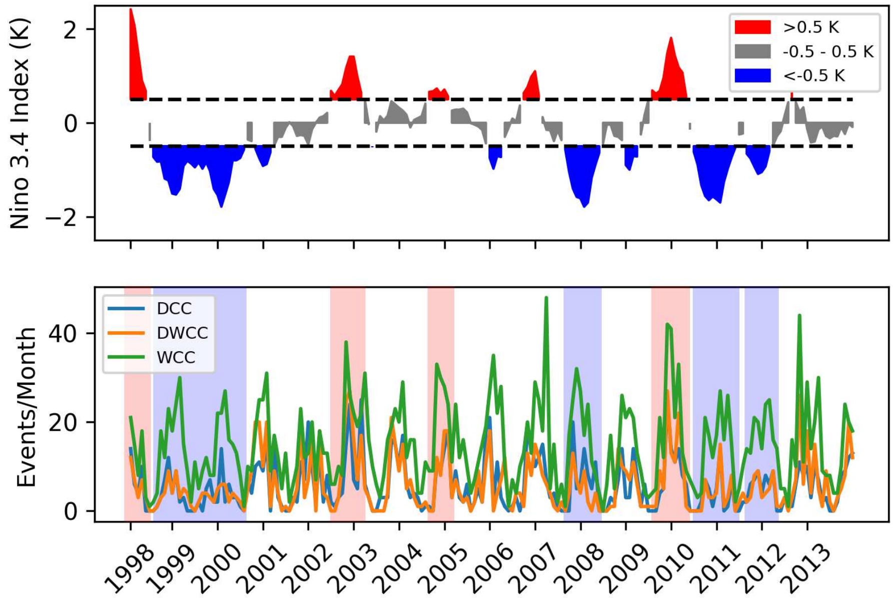

Figure 2.3: The Niño 3.4 index (upper panel) represents the temperature anomaly of the Niño 3.4 region. DCC, DWCC, and WCC events per month within the primary study regions are shown in the lower panel during the lifetime of TRMM, with color blocks representing the El Niño (red) and La Niña (blue) time periods, where the temperature anomalies last longer than six months.

ronments that occurred during these ENSO phases, synoptic composite differences are analyzed. Convective days are identified as days that contained any number of DCCs, DWCCs, and WCCs within the four primary study regions. It is important to note that high terrain may present challenges to reanalysis models in the lower levels of the atmosphere, specifically near the steep slopes of the Andes Mountains.

For convective days during El Niño in austral spring, a stronger surface lee cyclone is present compared to the El Niño climatology over the border of Bolivia, Paraguay, and Argentina (Fig. 2.4a). This anomalous low-pressure system may be an enhancement and displacement of the Northwestern Argentina Low (NAL), a climatological feature of this area (Lichtenstein 1980; Seluchi et al. 2003). The enhancement and displacement of this feature may promote stronger warm air and moisture advection, as well as improved orographic lift, through enhanced synoptic flow near the surface. At 850 hPa, increased moisture exists throughout the plains of subtropical South America, with a maximum increase in northeastern Argentina, for El Niño convective days

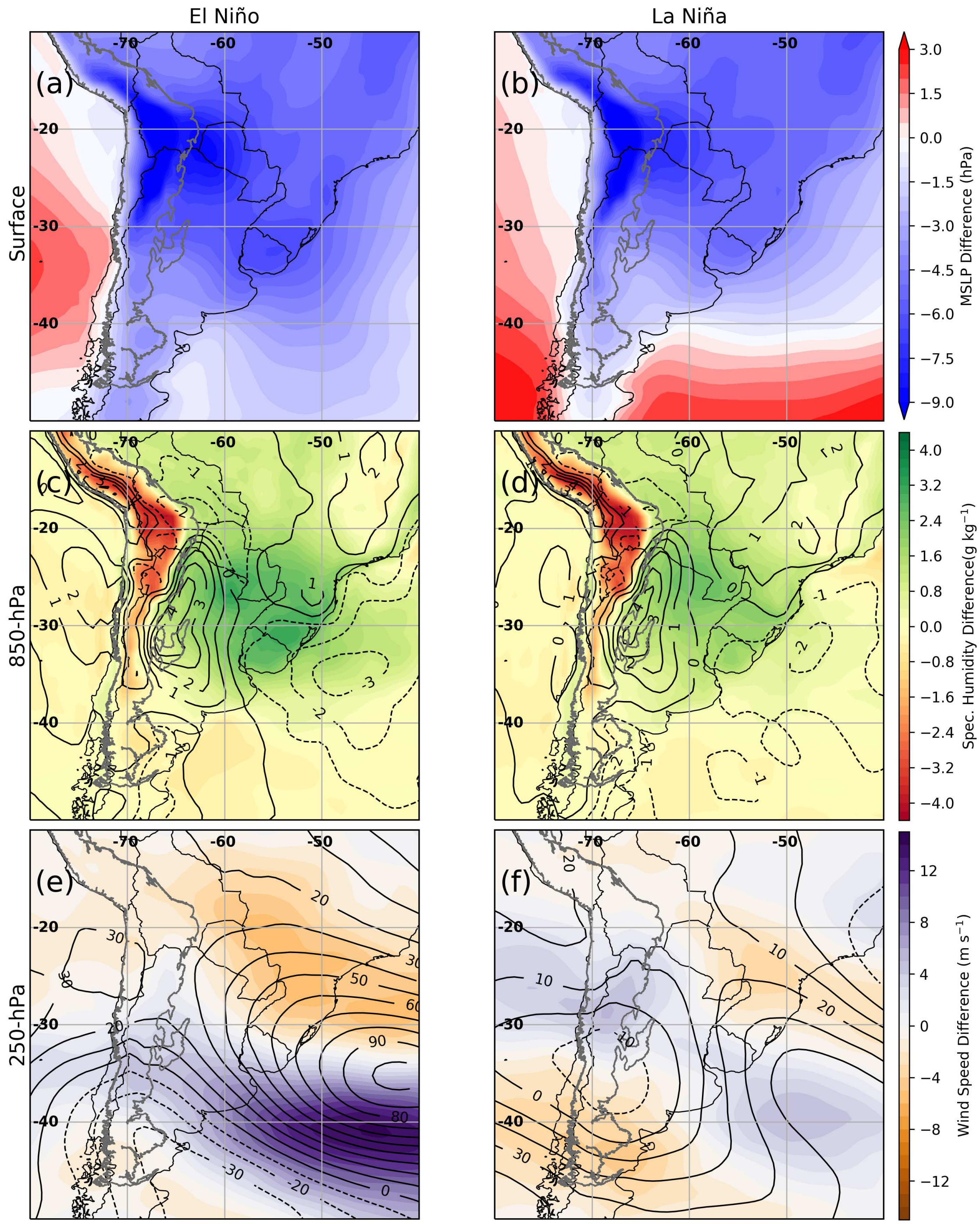

Figure 2.4: The differences between convective day composites and climatology during austral spring (SON) are shown for El Niño and La Niña. Convection had to occur within the four primary study regions in subtropical South America. Panels a and b show differences in mean sea-level pressure (MSLP), panels c and d map differences in 850-hPa specific humidity (filled) and meridional wind speed (contoured), and panels e and f display differences in 250-hPa wind speed and geopotential height.

compared to climatology (Fig. 2.4c). Northerly winds are reduced in magnitude during convective days, indicating a weaker low-level jet is present during these days as compared to climatology. However, at 250 hPa, the upper-level jet stream increases in strength during convective days from climatology by $6 - 9$ m s^{-1} (Fig. 2.4e). This anomaly is located in the same place as the climatological jet stream during El Niño (Fig. 2.4e), so this increase in wind speed during austral spring El Niño convective days represents an increase in the overall speed of the jet stream and not a latitudinal displacement of the jet stream. Increased jet strength would enable stronger secondary circulations, which would cause stronger rising motion over the primary study regions.

Similarly for La Niña, a stronger lee cyclone is present at the surface during austral spring convective days compared to climatology (Fig. 2.4b). Furthermore, moisture increases and meridional winds decrease at 850 hPa along the plains immediately east of the Andean foothills (Fig. 2.4d). However, at 250 hPa, the wind speed anomalies are not nearly as strong with increases of only $1 - 3$ m s^{-1} across subtropical South America (Fig. 2.4f). This difference would not substantially change the strength of the secondary circulations within the jet stream. The differences between convective days and climatology during austral summer are similar to the austral spring La Niña differences for both El Niño and La Niña (not shown).

If the convective days during El Niño and La Niña are compared, their influences on the synoptic environment in South America can be examined. Because composites were similar between storm types (not shown), all three categories of extreme convection were combined by ENSO phase to produce a single synoptic composite difference. At the surface, El Niño convective days are warmer than La Niña convective days in tropical South America and along the Andean foothills south to the SDC during austral spring but not summer (Fig. 2.5a, d). Rather, during summer, the 2-m temperature is cooler by about $1°$C in the central plains of Argentina. Farther south and east, El Niño convective days are cooler than La Niña convective days during both seasons. The dewpoint temperatures slightly increase during El Niño convective days compared to La Niña by $1°$C over northeastern Argentina, Uruguay, and southern Brazil (not shown).

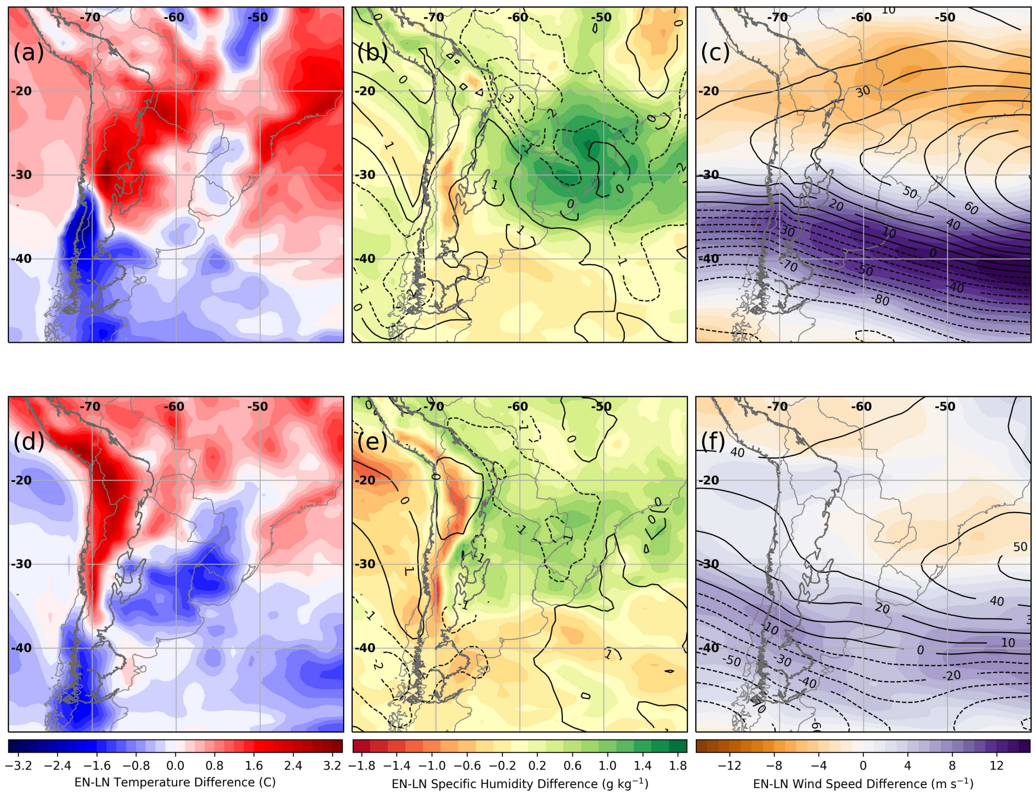

Figure 2.5: The differences between El Niño and La Niña convective days during austral spring (SON; panels a, b, c) and summer (DJF; panels d, e, f) are plotted for multiple vertical levels. Convection had to occur within the four primary study regions in subtropical South America. Panels a and d display the differences of 2-meter temperature. Panels b and e show the differences in 850-hPa specific humidity (filled) and meridional wind speed (contoured). Panels c and f plot the differences in 250-hPa wind speed (filled) and geopotential height (contoured).

At the 850-hPa pressure level, moisture increases by $1 - 1.5$ g kg^{-1} over northern Argentina, Paraguay, Uruguay, and southern Brazil on spring El Niño convective days as compared to La Niña convective days (Fig. 2.5b), while lesser increases in moisture are present on El Niño days during summer (Fig. 2.5e). Since flow is climatologically from the north (Fig. 2.5c, d), increases in meridional wind speed over Bolivia and Paraguay indicate a strengthening of the SALLJ, especially during spring. Over the primary study regions in subtropical South America, any changes in the strength of the SALLJ are negligible. At upper levels, though, the jet stream substantially increases in strength during El Niño as compared to La Niña on spring convective days (Fig. 2.5c), with only moderate increases in jet speed on summer El Niño convective days. Additionally, during El Niño convective days during both seasons, there is a stronger upper-level trough moving onshore across southern South America with a ridge downstream. The equatorward entrance region of the jet, favored for rising motion due to divergence at jet level, is located directly over the primary study regions. This enhanced upper-level support increases rising motion, which when coupled with topographic forcing along the SDC and Andean foothills, helps to overcome convective inhibition and cause the initiation of intense storms. Overall, the enhanced low-level moisture and upper-level jet stream supports a more favorable environment for convection during El Niño compared to La Niña, especially during austral spring.

2.4.2 Deep Convective Cores (DCCs)

Modest variations in DCC frequency do occur in different regions between ENSO phases, but DCCs occur across all phases of ENSO within the primary study regions in subtropical South America (Fig. 2.3 and Table 2.2). The largest differences in DCC frequency between El Niño and La Niña is in the SDC and SE sectors during austral spring and summer, which are statistically significant at the 90% confidence interval (Table 2.3). The SDC sector is the most active area for intense deep convection in subtropical South America, especially during austral spring and summer (Rasmussen et al. 2016). The eastern sectors have smaller frequency differences between El Niño and La Niña (Table 2.3).

Table 2.2: Total number of convective cores that occurred during an ENSO phase in a sector, divided seasonally into September, October, November (SON) and December, January, February (DJF).

	NW	SDC	NE	SE
El Niño				
DCC	16/13	34/74	18/12	29/29
DWCC	11/18	26/76	33/11	54/36
WCC	27/35	30/62	83/61	79/88
Neutral				
DCC	51/31	88/111	36/32	45/46
DWCC	59/30	61/106	55/25	83/58
WCC	63/94	77/151	109/74	158/160
La Niña				
DCC	19/12	31/49	21/16	25/21
DWCC	16/18	24/26	22/10	20/26
WCC	33/67	57/107	80/51	89/109

Table 2.3: Average number of the various convective cores that occur during an ENSO-phase month in a sector, divided seasonally as in Table 2.2.

	NW	SDC	NE	SE
El Niño				
DCC	0.53/0.43	1.13/2.47	0.60/0.40	0.97/0.97
DWCC	0.37/0.60	0.87/2.53	1.10/0.37	1.80/1.20
WCC	0.90/1.17	1.00/2.07	2.77/2.03	2.63/2.93
Neutral				
DCC	0.47/0.29	0.81/1.03	0.33/0.30	0.42/0.43
DWCC	0.55/0.28	0.56/0.98	0.51/0.23	0.77/0.54
WCC	0.58/0.87	0.71/1.40	1.01/0.69	1.46/1.48
La Niña				
DCC	0.35/0.22	0.57/0.91	0.39/0.30	0.46/0.39
DWCC	0.30/0.33	0.44/0.48	0.41/0.19	0.37/0.48
WCC	0.61/1.24	1.06/1.98	1.48/0.94	1.65/2.02

Using volumetric rain rates for each TRMM-identified storm in this study, DCC storms produce similar amounts of rain between El Niño and La Niña (Fig. 2.6). None of the sectors have a statistically significant difference between El Niño and La Niña. These storms only account for approximately 6% of the annual precipitation in this sector (Rasmussen et al. 2016); therefore, DCCs are not likely to account for the ENSO precipitation anomalies (Fig. 2.2a, b). The increased

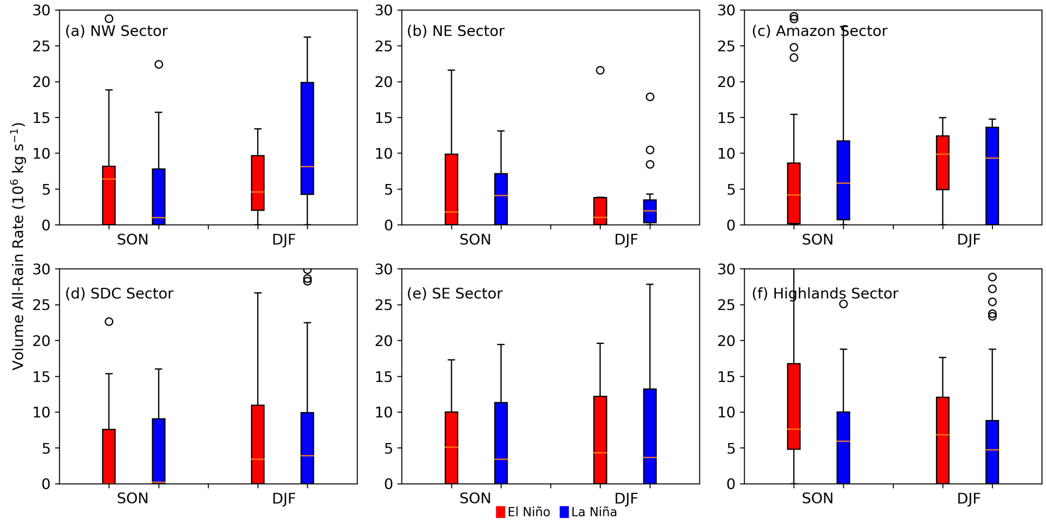

Figure 2.6: DCC volumetric rainfall by ENSO phase and sector in austral spring (SON) and summer (DJF) in a typical box-and-whiskers plot, where the open circles represent outlying data points. Statistically significant differences between El Niño and La Niña at the 95% confidence interval are represented by larger, hatched boxes.

rainfall rate in the Highlands sector during El Niño agrees with the findings of Grimm and Tedeschi (2009). The Amazon sector shows heavier rain rates during La Niña in austral spring, although the differences in rainfall rates are not statistically significant in this study.

One of the most substantial and statistically significant differences in DCCs between ENSO phases is in the maximum convective core height, calculated as the maximum height of the 40-dBZ contiguous echo core. Across almost all seasons and sectors, El Niño DCCs are taller than La Niña DCCs (Fig. 2.7). The maximum height differences between ENSO phases are statistically significant at the 95% confidence interval during spring in all four sectors and during summer in the SDC sector. These differences indicate that more vigorous deep convection occurs during El Niño, as storms are frequently $1-2$ km taller during El Niño than La Niña.

A useful tool in diagnosing storm characteristic differences between ENSO phases in the TRMM PR data is the CFAD diagram described in subsection 2.2. The entire storm that contains the DCC is analyzed, thus convective and stratiform rainfall is included in the CFAD results. The difference between the El Niño and La Niña convective CFADs confirms that El Niño DCCs have more robust and deeper convection, with a shift in the distribution of echoes toward higher

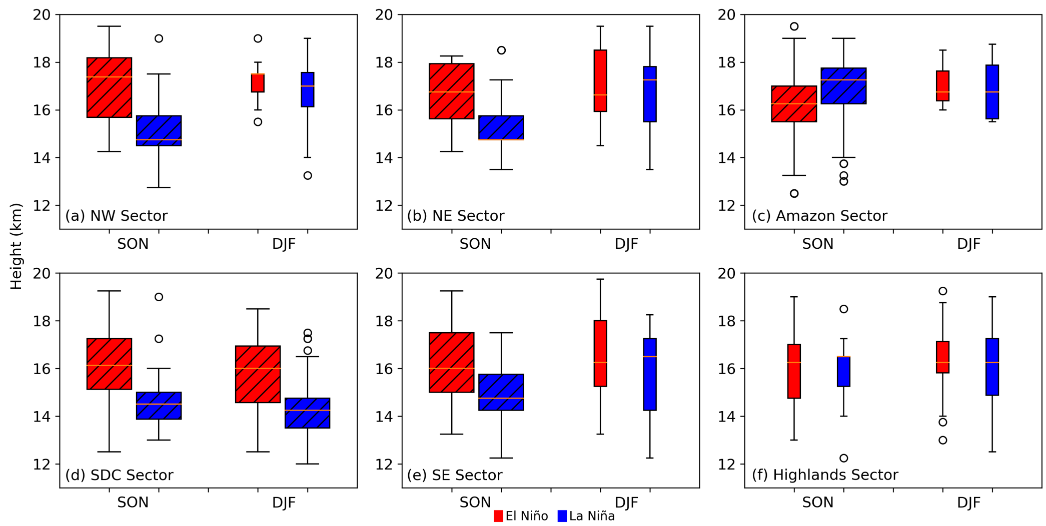

Figure 2.7: Same as Figure 2.6, but for the maximum height of the contiguous convective core.

reflectivities within El Niño DCCs (Fig. 2.8a). In the stratiform CFAD, enhanced stratiform pre-

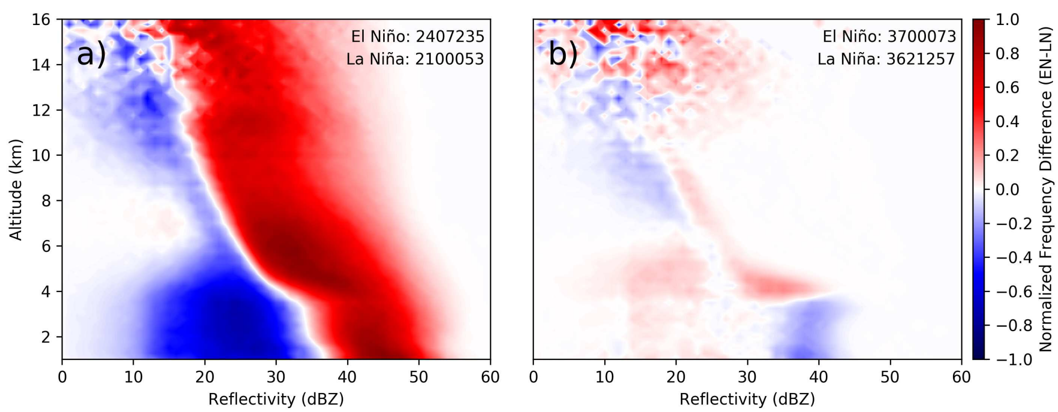

Figure 2.8: Differences between El Niño and La Niña Contoured Frequency by Altitude Diagram (CFADs; Yuter and Houze 1995) for DCCs, separated by convective (panel a) and stratiform (panel b) rain with each vertical level normalized by the most frequent reflectivity bin within that level. Positive values represent an increase in frequency for storms during El Niño. The number of pixels that went into each composite are listed in the top right corner of each panel.

cipitation below the melting level is evident during La Niña, with more frequent echoes near 40 dBZ between $0 - 4$ km (Fig. 2.8b). Given that the volumetric rain rates are fairly similar for both El Niño and La Niña DCCs (Fig. 2.6), the reduced convective intensity and increased stratiform intensity near the surface likely balances out and results in a fairly similar total rainfall amount, but from different types of precipitation echoes. This result is supported by additional analysis showing that the area of the stratiform precipitation is similar between ENSO phases (not shown).

ENSO also modifies the synoptic environment which supports deeper convective storms during El Niño (Figs. 2.4, 2.5). While differences in the synoptic environment associated with El Niño and La Niña were discussed earlier, a more detailed look at changes to instability yields new insights. Convective available potential energy (CAPE) is often used as a forecasting metric to quantify potential storm intensity. ERA-Interim reanalysis composite differences between El Niño and La Niña show an increase in surface-based CAPE in all sectors during El Niño (Fig. 2.9). This

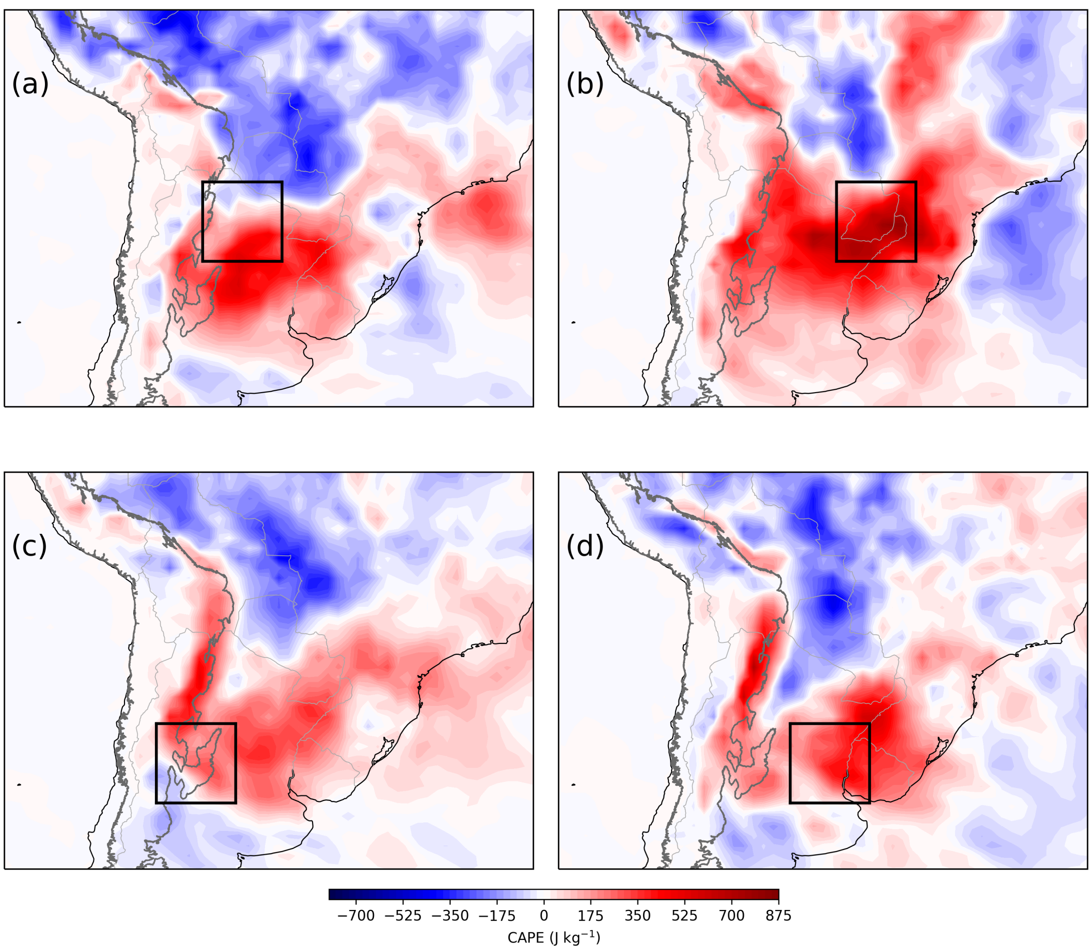

Figure 2.9: Difference in SB-CAPE (J kg^{-1}) between El Niño and La Niña for days with storms in each of the sectors outlined in black.

enhanced thermodynamic support allows for deeper and stronger convection, with greater vertical motion throughout the storm. The greatest increase in CAPE during El Niño occurs when DCC storms are in the SE sector. When storms occur in the two western sectors, the maximum increase in CAPE is not centrally situated within their regions, but there is still a net increase in CAPE within each sector.

2.4.3 Deep and Wide Convective Cores (DWCCs)

Deep and wide convective cores (DWCCs) occur in similar frequency as DCCs (Tables 2.2, 2.3). DWCCs are most frequent within the southern sectors for all seasons and ENSO phases. During El Niño, DWCCs occur most frequently during austral summer in all sectors. Additionally, they are more frequent in the eastern sectors during El Niño than La Niña. These storms produce heavy rainfall, which causes flash and slow-rise flooding if they remain stationary for many hours.

The storm characteristics of DWCCs occurring during the two ENSO phases are compared in Figures 2.10 and 2.11. Rainfall resulting from DWCCs are similar during El Niño and La Niña

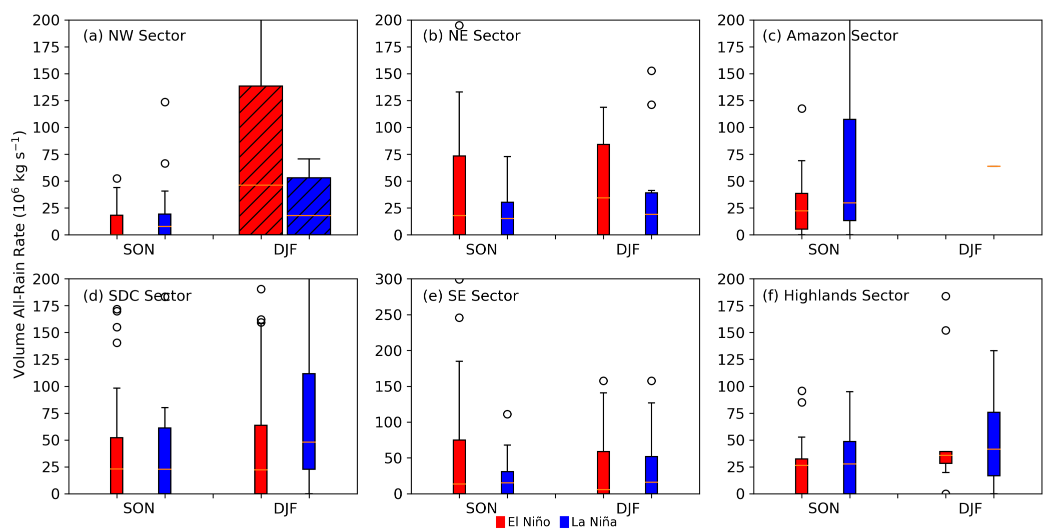

Figure 2.10: Same as Figure 2.6, but for the rainfall rates found in DWCCs.

phases, with the only statistically significant difference occurring in the NW sector during summer (Fig. 2.10). Similar to the results for the DCCs, DWCCs are also deeper during El Niño in the

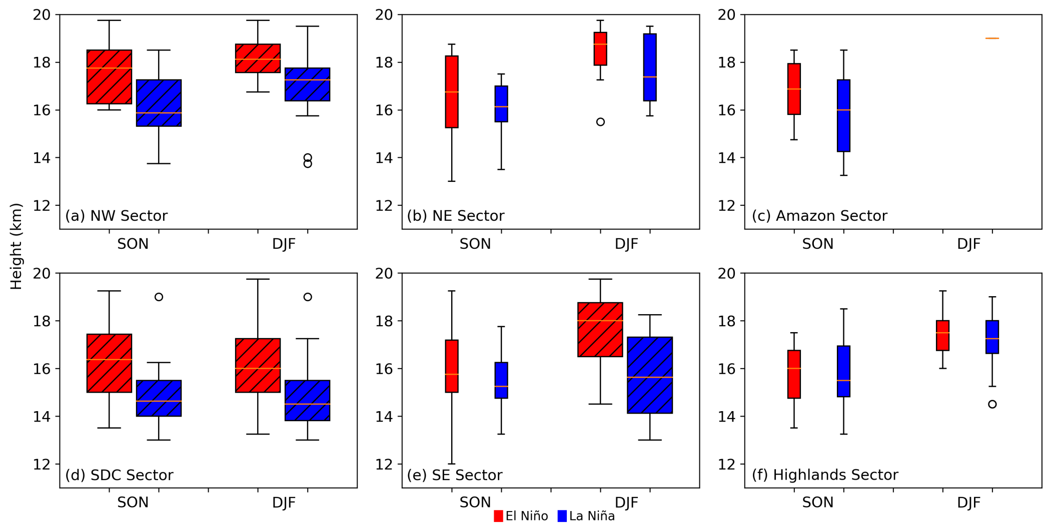

Figure 2.11: Same as Figure 2.7, but for the maximum height of DWCCs.

subtropical sectors across almost all seasons (Fig. 2.11). The height differences are statistically significant at the 95% confidence interval for the NW, SDC, and SE sectors during spring and NW and SDC sectors during summer. In the Amazon and Highlands sectors, the results are mixed due to limited numbers of storms in these areas.

The difference between the CFADs for DWCCs during El Niño periods and La Niña periods are shown in Figure 2.12 for both the convective and stratiform components of the storms containing DWCCs. The convective difference CFAD shows a strong shift toward higher reflectivity at all

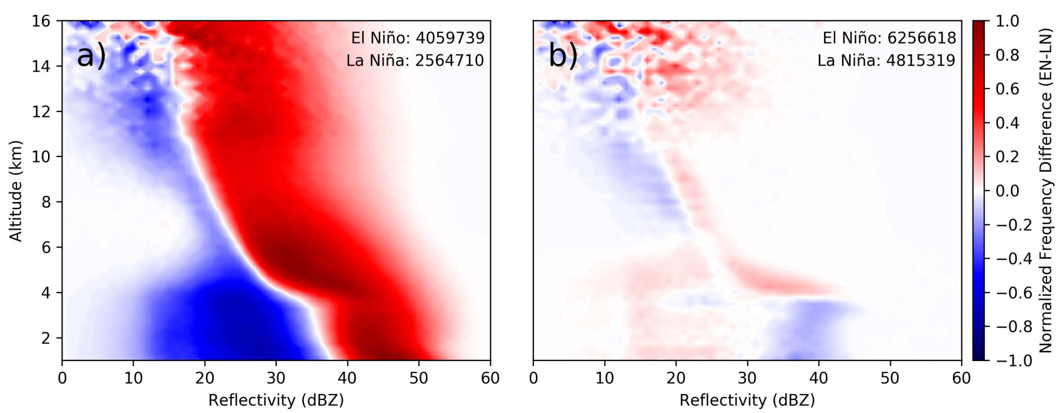

Figure 2.12: Same as Figure 2.8, but for CFADs of DWCCs.

levels during El Niño periods, indicating more intense convection throughout the entire depth of the storm (Fig. 2.12a). Combined with the taller height of the 40-dBZ core shown previously (Fig. 2.11), DWCCs appear to be more intense during El Niño. Within the stratiform region of El Niño DWCCs, there is a shift to higher reflectivites above the bright band at 4 km which indicates enhanced stratiform precipitation aloft (Fig. 2.12b). However, below the bright band, La Niña DWCC storms have higher reflectivities than El Niño DWCCs.

As was seen for DCC storms (Fig. 9), these deeper and stronger DWCC storms have as much as $500 - 700$ J kg^{-1} higher values of CAPE during El Niño compared to La Niña (Fig. 2.13). No

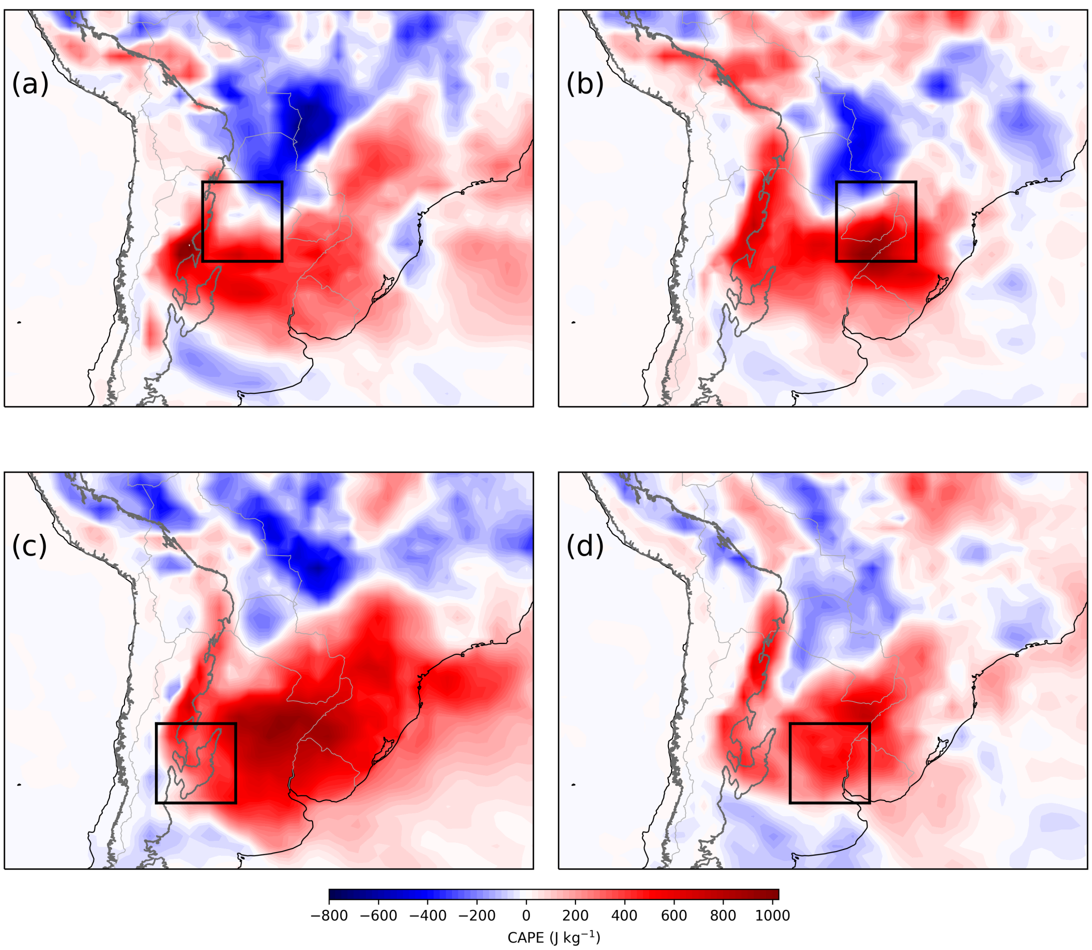

Figure 2.13: Same as Figure 2.9, but for CAPE on days with DWCCs.

matter which sector the DWCC storm occurs in, there is an increase in CAPE during El Niño along the Andean foothills and SDC. These increases in instability would support convective initiation over the topography once any capping inversion is broken (Rasmussen and Houze 2016).

2.4.4 Wide Convective Cores (WCCs)

Wide convective cores (WCCs), which represent upscale-organized and mature MCSs capable of producing heavy rainfall and flooding (Houze et al. 2007; Rasmussen and Houze 2011), are the most frequent type of intense convection in all study regions and seasons (Tables 2.2, 2.3). The two eastern sectors have the highest frequency of WCC occurrence for all ENSO phases due to the tendency for storms to grow upscale as they move eastward following initiation (Romatschke et al. 2010; Rasmussen and Houze 2011, 2016). With respect to ENSO, WCCs are more frequent during La Niña in all sectors and seasons, with the exception of the NE sector during austral summer. The SE sector generally has the greatest frequency of WCCs (Table 2.3), and the differences in frequency in this sector between El Niño and La Niña are statistically significant at the 90% confidence interval. In the western sectors, WCCs are most common during austral summer (Tables 2.2, 2.3).

The mean volumetric rainfall rates appear almost identical between ENSO phases for all sectors, with no statistically significant differences (Fig. 2.14). Therefore, if a WCC occurs, it likely produces similar volumetric rainfall rates regardless of the ENSO phase. Storm duration is not analyzed in this study due to the nature of the TRMM satellite's orbit in capturing storm snapshots; therefore, total rainfall amounts and the climatological rainfall anomalies cannot be analyzed from this perspective. It is possible that changes in storm duration, broad stratiform regions (Houze et al. 2007), or non-extreme precipitation differences between ENSO phases may account for the climatological rainfall anomalies (Fig. 2.2a, b), but is beyond the scope of the current study.

Examining the maximum height of the convective core, El Niño WCCs tend to be taller than La Niña WCCs, especially in the NE and SDC sectors (Fig. 2.15), but the magnitude of the difference is usually less than one kilometer. The differences are statistically significant at the 95%

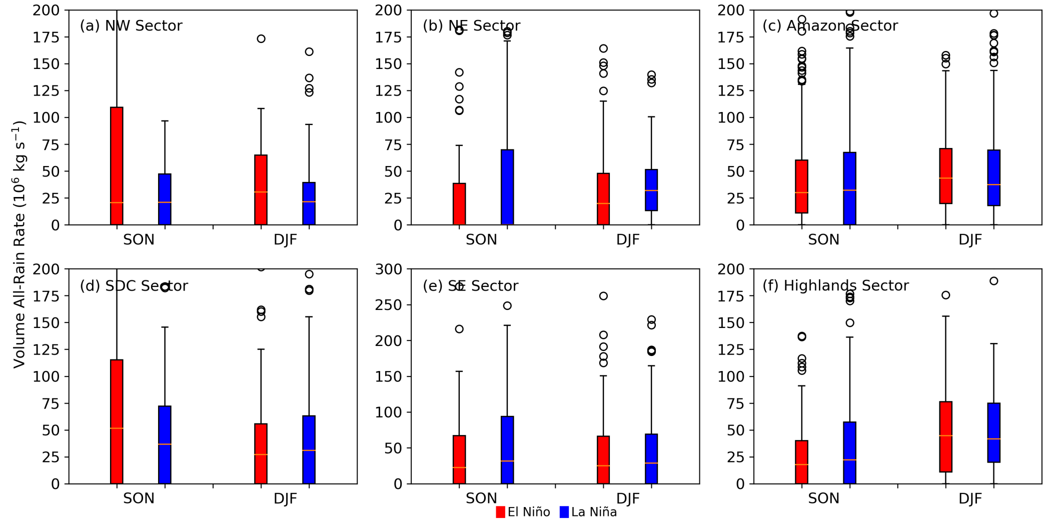

Figure 2.14: Same as Figure 2.6, but for the rainfall rates found in WCCs.

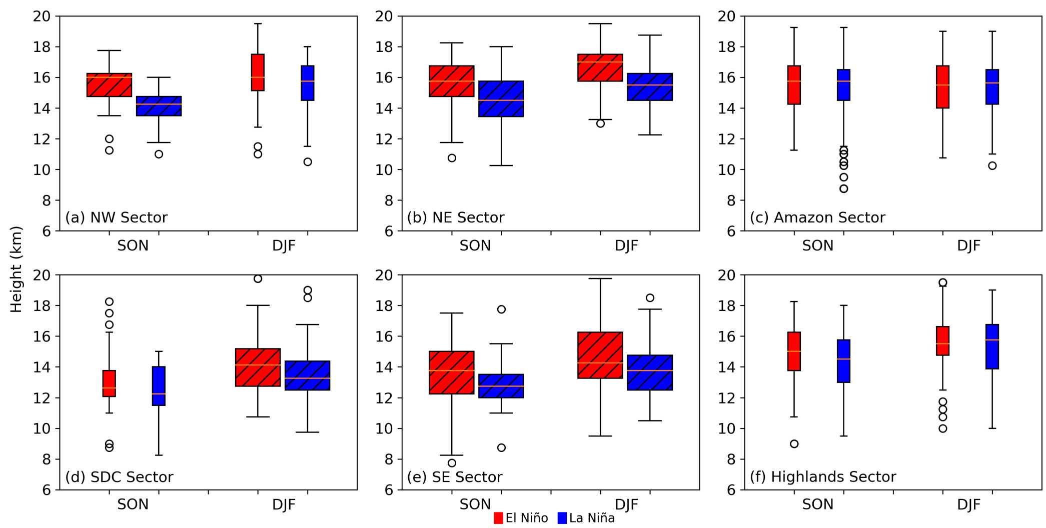

Figure 2.15: Same as Figure 2.7, but for the maximum height of WCCs.

confidence interval during spring and summer in all subtropical sectors except for the SDC sector during spring and the NW sector during summer. Since all three categories of intense convection are deeper during El Niño, this appears to be a systematic difference in convection during the warm phase of ENSO.

Increased frequencies of higher reflectivities during El Niño is apparent in the convective CFAD, indicating that WCCs contain more frequent strong convection during El Niño compared to La Niña (Fig. 2.16a). The bright band does not appear to be stronger during a particular ENSO

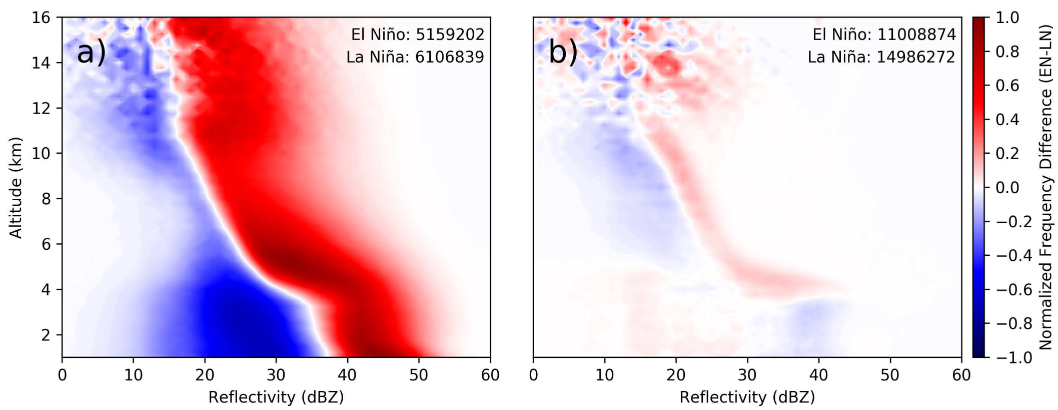

Figure 2.16: Same as Figure 2.8, but for CFADs of WCCs.

phase in the stratiform CFAD (Fig. 2.16b). As a result, there are minimal differences in the stratiform structure of WCCs between ENSO phases. Therefore, it appears that once a storm has grown upscale into a WCC, rainfall intensities are similar in El Niño and La Niña conditions.

The analysis of thermodynamic conditions for WCCs helps explain why they tend to be deeper and contain stronger convection. Surface-based CAPE is greater in all sectors during El Niño than La Niña, although the magnitude is small ($100 - 300$ J kg^{-1}; Fig. 2.17). Greater CAPE would support enhanced updraft speeds and more convective initiation once any convective inhibition is removed.

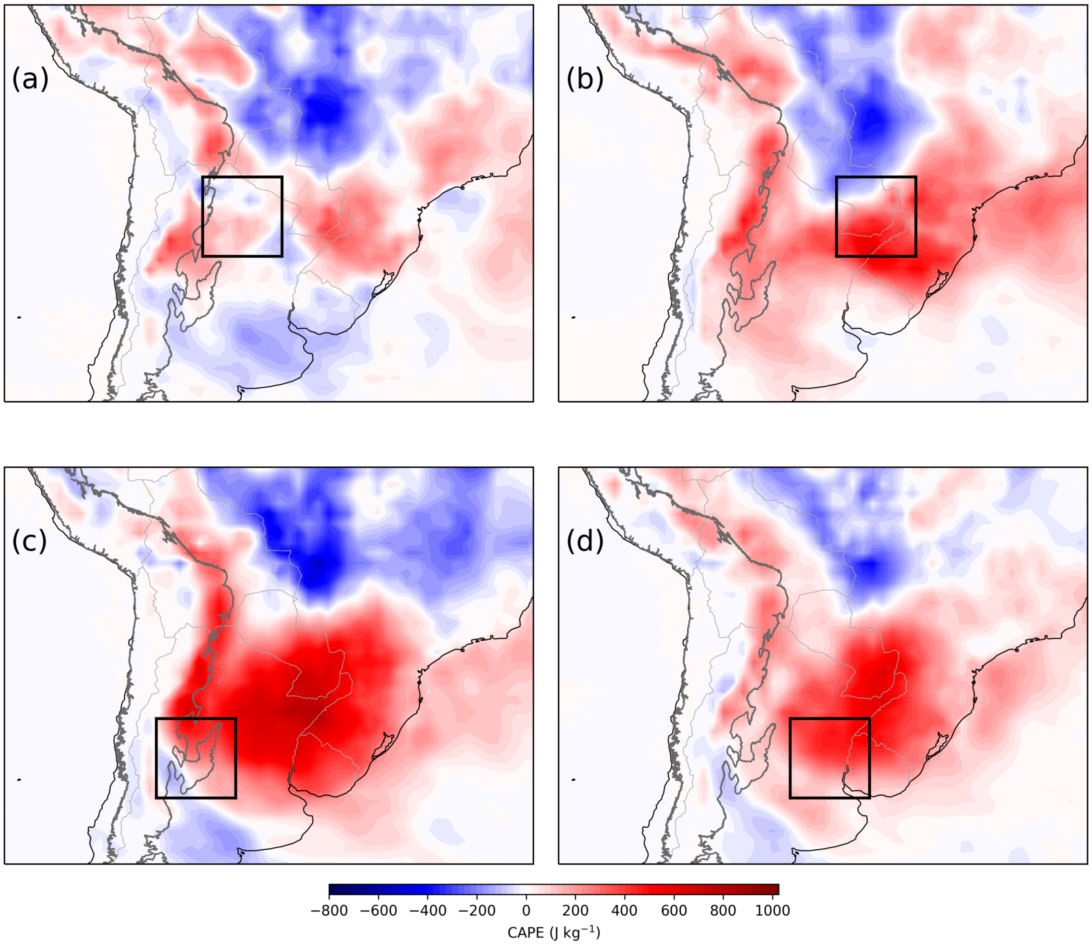

Figure 2.17: Same as Figure 2.9, but for CAPE on days with WCCs.

2.4.5 Summary

Overall, DCCs, DWCCs, and WCCs tend to be deeper and contain stronger convection during El Niño compared to La Niña. Increased CAPE and favorable placement of the equatorward entrance region of the jet stream support these stronger storms. While more rain falls in the eastern sectors climatologically during El Niño, this study found similar rainfall rates between ENSO phases from these intense convective storms. With stronger storms occurring during El Niño, more hazardous weather may occur, such as hail and high winds. However, storm frequency does not vary greatly, and subtropical South America is likely to see DCCs, DWCCs, and WCCs in all phases of ENSO with varying storm characteristics.

2.5 Conclusion

Convection is an important component of Earth's climate; thus, it is critical to understand how large-scale atmospheric variability affects the frequency and intensity of convection. The variability of convection causes hydrologic extremes, such as flash flooding and drought, and modulate the frequency of severe weather. This study examines how ENSO conditions influences the frequency and characteristics of extreme convective storms in subtropical South America using a 16-year TRMM PR dataset and ERA-Interim reanalysis.

While previous research found that El Niño may suppress convection over tropical South America (Liebmann and Marengo 2001; Espinoza Villar et al. 2009; Shimizu et al. 2017), this study found that different phases of ENSO did not significantly promote or inhibit intense convection in the lee of the Andes Mountains, but more importantly modulated its frequency and strength. Deep convective storms (DCCs) tend to be more common during El Niño near the terrain in the foothills of western Argentina in austral spring and summer, while wide convective cores (WCCs) tend to be more frequent during La Niña in most sectors and seasons. Although this study found that rainfall increases during El Niño in the eastern subtropics of South America, the cause of these anomalies is not analyzed in this study. Changes in storm frequency and duration, along with changes to non-extreme precipitation, may explain the climatological ENSO precipitation anomalies and will be analyzed in future work. This study also does not explain why there is an increased frequency of WCCs during La Niña and may be the focus of a future study.

During El Niño, intense convective storms tend to be taller and contain more intense convective precipitation aloft than storms during La Niña. However, La Niña DCCs and DWCCs have enhanced stratiform reflectivities below the melting level, leading to more intense rainfall within those regions of the storms. Synoptic support for taller and more intense DCCs, DWCCs, and WCCs during El Niño likely comes from enhanced CAPE and favorable placement of the equatorward entrance region of the jet stream, which supports vertical motion through its secondary circulation. More moisture is also available to these storms within the primary study regions in subtropical South America. Overall, these enhanced synoptic conditions for convection are similar to the climatological changes in the synoptic environment that occur during El Niño (Fig. 2.4).

The results herein demonstrate that subtropical South America supports convection in any phase of ENSO and that the variability of extreme convection within this region does not appear to be strongly tied to ENSO, unlike some other regions of the world. As a result, seasonal-to-subseasonal forecasting of subtropical South American convection based on ENSO patterns is unlikely to improve upon climatological forecasts. Small variations between phases cause intense convection to be stronger or weaker at different times, but the variability of high-impact severe weather hazards between ENSO phases, such as large hail or flooding, is beyond the scope of the current study. Finally, these results show that the economic sectors most at risk from hazardous convective storms do not realize a reprieve from strong convection during a particular ENSO phase, but may experience rainfall extremes depending on the phase.

Chapter 3

Subtropical South American Hailstorm Characteristics and Environments

Hailstorms in subtropical South America are known to be some of the most frequent and powerful anywhere in the world, causing significant damages to the local agricultural economy every year. Convection in this region tends to be orographically-forced, with moisture supplied from the Amazon rainforest by a low-level jet. Previous climatologies of hailstorms in this region have been limited to localized and sparse observational networks. Due to the lack of sufficient ground-based radar coverage, objective radar-derived hail climatologies have also not been produced for this region. As a result, this study uses a 16-year dataset of TRMM Precipitation Radar and Microwave Imager observations to identify possible hailstorms remotely, using 37-GHz brightness temperature as a hail proxy. By combining instruments and reanalysis modeling, this study produces the first objective study of hailstorms in this region. Hailstorms in subtropical South America have an extended diurnal cycle, often occurring in the overnight hours. Additionally, they tend to be multi-cellular in nature, rather than discrete. High-probability hailstorms tend to be deeper and horizontally larger than storms have a low-probability of containing hail. Finally, hailstorms are supported synoptically by strong upper- and lower-level jets, anomalously warm and moist low levels, and enhanced instability. The findings of this study will support the forecasting of these dangerous storms and mitigation of their damages within this region.

3.1 Introduction

Hail in subtropical South America is extremely large (> 5 cm; Rasmussen et al. 2014) and frequent (Cecil and Blankenship 2012) and causes significant impacts to property and the agricultural economy in this region. Hail has been studied for more than five decades, yet relatively little is known about the storms that produce hail or the environments that support hail-producing storms in subtropical South America. Hail research in this area goes back to the 1960s, when hail mitigation experiments began near Mendoza, Argentina (Grandoso and Iribarne 1963). Hail observations were extremely limited at this time, but some frequency of hail was noted near the Atlantic coast and the Andes Mountains (Frisby and Sansom 1967; Williams 1973). More recent mitigation work has continued in the Mendoza area to reduce hail risk to wineries (Makitov 1999) and to study the time series of hail events (Prieto et al. 1999). Large hail ($>$ 2 cm) was found to cause 80% of the agricultural damages in the Mendoza region through only 2-3 events annually (Perez and Puliafito 2006). An in-depth study of hailpad observations was undertaken by Sanchez et al. (2009), which compared the hailpad climatologies of Mendoza to regions in France and Spain. This study found that the network in Argentina was found to have a greater frequency of large hailstones than those in Europe.

The most thorough report-based hail climatology for subtropical South America used weather station observations of hail to produce an interpolated gridded hail frequency (Mezher et al. 2012). This study highlighted two main areas of frequent hail: 1) Mendoza, extending east towards Córdoba and the central plains of Argentina, and 2) Patagonia. This southern region of hail activity may be a result of graupel being counted as hail in this colder region of the continent. Mezher et al. (2012) also found that hailstorms tend to occur when there are warm temperature anomalies near the surface and cold anomalies in the upper atmosphere, leading to the creation of an unstable atmosphere. While this study produced a national hail climatology over an extended time period, it was limited to surface station observations, which are relatively sparse across the region and must be reported by an observer. Ground-based radar-derived hail climatologies, such as those conducted in the U.S. (e.g., Pocakal et al. 2009; Cintineo et al. 2012), are unable to be produced in subtropical South America due to the very recent installation of ground-based radar networks in Argentina. With time, this will be a promising avenue to explore hail within this region, but currently the data record is not extensive enough for a thorough analysis.

As a result, the most comprehensive way to examine the climatology of hail in subtropical South America, and compare these results to other parts of the world, is to use passive microwave satellite observations of ice hydrometeors. These measurements have been shown to be well-calibrated to large hail reports (1 inch or greater diameter) within the U.S. (Cecil 2009), which has allowed their use in producing global climatologies of hailstorms and intense convection (Cecil and Blankenship 2012). These studies found intense convection with likely hail production, and specifically maxima in hail frequency, in the lee of major mountain ranges that is consistent with spaceborne radar-based climatologies of deep convection (Zipser et al. 2006; Houze et al. 2015). These findings also correspond well with recent observational work in Canada (Smith and Yau 1993; Etkin and Brun 2001), Croatia (Pocakal et al. 2009), China (Zhang et al. 2008), and Argentina (Mezher et al. 2012). However, the frequencies of large hail within these different regions show a large degree of variability. Comparing the foothills of the Rockies to the foothills of the Andes, there is an order of magnitude increase in the frequency of hail in the subtropical South American region (Cecil and Blankenship 2012). The reason for this difference between hail frequencies in close proximity to major mountain ranges is not well-understood.

Meanwhile, examination of extreme convection using the Tropical Rainfall Measuring Mission (TRMM) satellite's Precipitation Radar (PR) showed that subtropical South America has some of the most extreme deep convection anywhere in the world (Zipser et al. 2006; Houze et al. 2015). This convection tends to be orographically-favored, with warm and moist air supplied by the South American low-level jet (SALLJ) from the Amazon, and convective inhibition through mechanical subsidence in the lee of the Andes (Rasmussen and Houze 2011, 2016). These storms remain close to the terrain, back-building over time (Rasmussen et al. 2014). Even as stratiform precipitation develops downstream, deep convection often remains tied to the terrain, where constant orographic lift and moisture convergence enables maintenance of strong convection. Additionally, these extreme storms have been linked with the production of severe hazards, including hail, tornadoes, and flash flooding (Rasmussen et al. 2014), but the lack of an extensive storm report database in this region prevents an in-depth collocation of the TRMM PR dataset with storm reports.

Therefore, this study seeks to combine TRMM PR and radiometer measurements to examine the diurnal and annual cycle, storm characteristics, and synoptic environments of hailstorms in subtropical South America. The results of this study will improve the understanding of how, why, and when hailstorms form and what characteristics may differentiate them from convection that does not produce hail. Through this analysis, a more comprehensive understanding of the climatology of hail and hail-producing environments will be presented. The results from this study will provide context for the results of the RELAMPAGO field campaign . Finally, this study will contribute to a better global understanding of hailstorms to help improve forecasting and diagnosis of hailstorms in subtropical South America.

3.2 Methodology

Due to the lack of a hail report database in subtropical South America, satellite measurements of ice scattering serve as sufficient proxies for analyzing convection that may support the production of hail (Cecil 2009; Cecil and Blankenship 2012). Using the methods established in Cecil and Blankenship (2012), 16 years of data (1998-2013) from the Tropical Rainfall Measuring Mission (TRMM) satellite were used. The Precipitation Radar (PR) and TRMM Microwave Imager (TMI) were utilized to identify convection and determine the probability that it contains hail. The TRMM satellite orbited the tropics between $36°$N and $36°$S from 1997-2014 (Kummerow et al. 1998). The TRMM PR had a resolution of $4 - 5$ km horizontally and 250 m vertically, while the TMI had a resolution of 16 km by 9.7 km for the 37-GHz channel (Kummerow et al. 1998, 2000). The 37-GHz channel is the best frequency on the TMI to discriminate whether convection is likely to produce hail (Cecil 2009), as this channel maximizes detection while minimizing false alarms. It is important to note that this method of hail identification is unable to distinguish hail size, as the satellite is only able to detect the volume of large ice particles within a storm.

While TMI deciphers whether a storm is likely to contain hail, it does not provide information about the three-dimensional characteristics of the storm. As a result, colocated TRMM PR data is used to provide details about hailstorm structure. Two TRMM data products are used in this study:

- 2A23 (rain characteristics; Awaka et al. 1997), where TRMM orbital precipitation data is separated into the three categories of convective, stratiform, and other.

- 2A25 (rainfall rate and profile; Iguchi et al. 2000), which contains the TRMM orbital three-dimensional attenuation-corrected reflectivity data.

To focus this study on hail-producing convection in subtropical South America, a study area was defined that includes the primary region of intense convection and satellite-derived climatological hail maximum (Fig. 3.1; Cecil and Blankenship 2012; Rasmussen et al. 2014, 2016). The

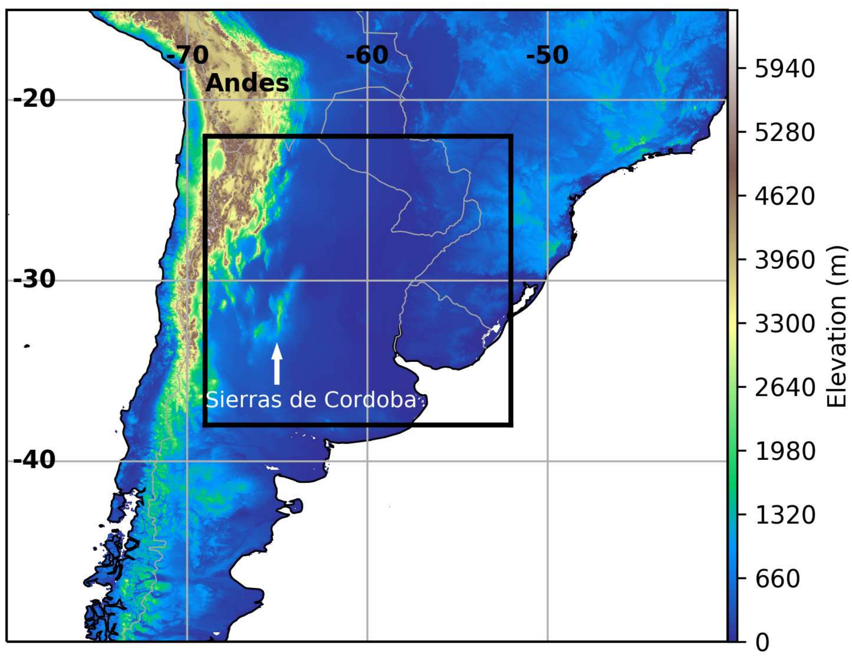

Figure 3.1: South America with topography and the study area outlined.

study area includes the Andean foothills and Sierras de Cordoba (SDC), which are hypothesized to be an orographic trigger for convective initiation (Rasmussen and Houze 2011, 2016), due to the impingement of the South American low-level jet (SALLJ) on the topography. The orographic forcing helps to overcome any mechanical capping produced by subsiding upper-level air in the lee of the Andes. Additionally, the SDC and the plains immediately to their east are the focus of the RELAMPAGO field campaign, which was conducted during November and December 2018.

In order to understand the lifecycle of intense convection, the TRMM PR data were separated into three categories, including deep, deep and wide, and wide convective cores (DCCs, DWCCs, and WCCs, respectively) following the methodology established by Houze et al. (2007) and Romatschke and Houze (2011). DCCs are defined as convection that has a contiguous three-dimensional 40-dBZ echo above 10 km, WCCs are storms that have a contiguous 40-dBZ echo over 1000 km^2, and DWCCs, are convection that meet the criteria to be both DCCs and WCCs. All three categories are mutually exclusive, such that there is no overlap between them. DCCs and DWCCs represent the most intense deep convection, while the DWCCs and WCCs are indicative of mesoscale convective systems, which are large, well-organized, mature convective storms (Houze 2004). This methodology has been used in many previous studies on convective storm characteristics around the world (Rasmussen et al. 2014, 2016; Rasmussen and Houze 2011, 2016; Zuluaga and Houze 2015).

The 37-GHz polarization-corrected brightness temperatures (PCT; Cecil and Chronis 2018) from TMI are analyzed to assign probabilities that DCCs, DWCCs, and WCCs contained hail. Correcting the brightness temperatures based on the differences between the polarized channels allows for discrimination between surface water features and ice scattering within convection. The probability that a storm contained large hail is based on the methodology from Cecil and Blankenship (2012). If the storm had a 37-GHz PCT greater than 200 K, it was considered to have a low probability of hail and designated as a null case in this study. Storms with 37-GHZ PCT between $176 - 200$ K were considered to have medium probability of hail; those thresholds correspond to between $25 - 50\%$ likelihood of large hail being reported in the U.S. Storms with 37-GHz PCT below 176 K have a high probability of producing large hail. These classifications based on 37-GHz PCT allowed for investigation into differences between storms with different probabilities of containing hail.

Finally, synoptic environments for each storm were analyzed with ERA-Interim reanalysis data (Dee et al. 2011). All maps use the 18 UTC (15 LT for Argentina) time for the composite, which was composed of days when storms occurred after 12 UTC or the day prior if the storms occurred between before 12 UTC. Days were binned by hail probability category (high, medium, or null) based upon the maximum hail probability that occurred during each day.

3.3 Results

3.3.1 Annual and Diurnal Cycles

During the 16-year observational period, a large number of storms were captured by the TRMM satellite (Table 3.1). DWCC storms contained the greatest percentage of potential hailstorms

Table 3.1: The breakdown of storms identified within the study area by storm type and hail probability.

	DCC	**DWCC**	**WCC**
High-probability	167	364	79
Medium-probability	215	425	266
Null	919	399	2546

(66.4%), per the probabilities calculated from 37-GHz PCT. 29.4% of DCCs were potential hailstorms, while only 11.9% of WCCs qualified under these metrics. The annual cycle of hailstorms in this region is similar to that in the U.S. (Allen and Tippett 2015), with the maximum frequency of hail occurring during the austral warm season (October through March; Fig. 3.2). Hailstorm activity begins to increase during September, reaches a fairly steady frequency from October through March, and the frequency decreases in April with reduced hail activity during the austral winter. These results match well with the annual cycle found by Mezher et al. (2012) in their E and H regions, which cover central and northwestern Argentina, respectively.

An examination of the diurnal cycle of hailstorms demonstrates the unique nature of these storms in subtropical South America (Fig. 3.3). Hailstorm activity begins to increase early in the afternoon (17 UTC; 14 LT) and continues through the next morning. This diurnal cycle is significantly extended into the nocturnal hours compared to the U.S., where hail is infrequent after midnight (Allen and Tippett 2015). Cecil and Blankenship (2012) noted a broad peak between 15-00 LT for subtropical South America, with a slow decline in activity through the morning hours. This contrasted with sharp declines after 9 pm LT for all other regions with high hail frequencies in their study - the U.S., central Africa, Pakistan, and Bangladesh. The high-probability

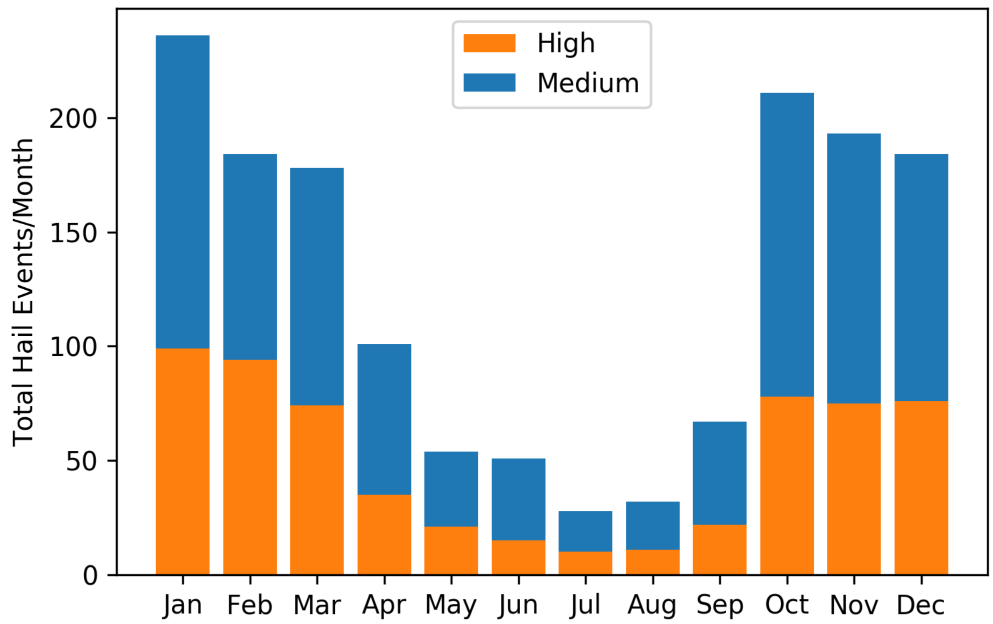

Figure 3.2: The annual cycle of hailstorms within the study area as a stacked bar graph of high- and medium-probability hailstorms.

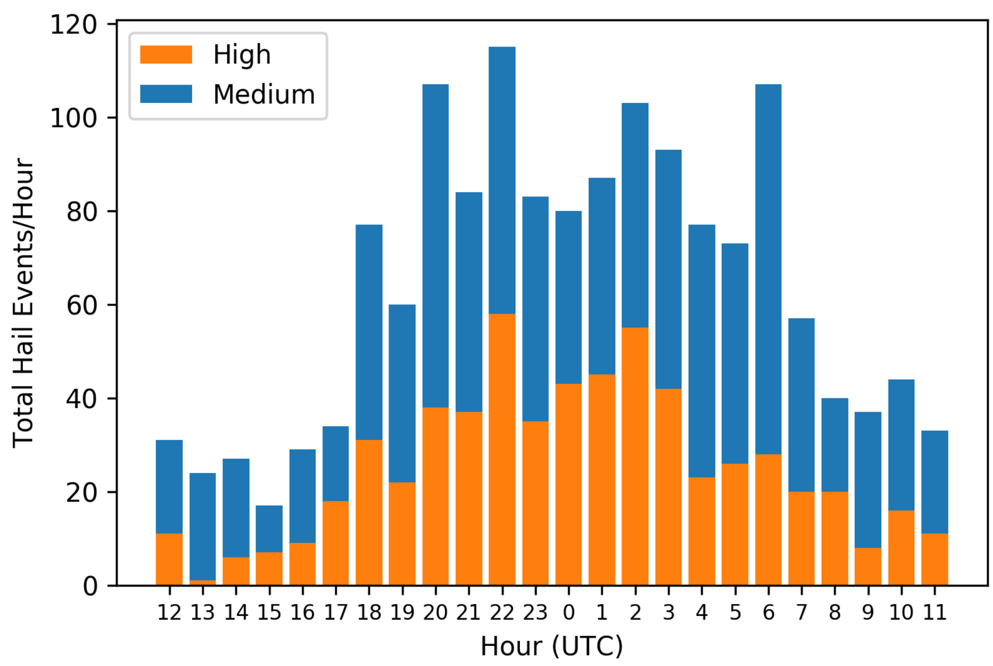

Figure 3.3: The diurnal cycle of hailstorms within the study area as a stacked bar graph of high- and medium-probability hailstorms.

storms in Fig. 3.3 have their maximum frequency from 20 to 03 UTC (5 pm to 12 am LT). For medium-probability events, the period of maximum frequency extends through 06 UTC (3 am). This enhanced frequency of hail during the overnight hours is a unique feature of subtropical South America, which has also been anecdotally observed via social media reports.

Breaking the diurnal cycle down by storm type, high-probability hail-producing DCCs and DWCCs have similar diurnal cycles, with their primary frequency peak during the late afternoon and evening hours (Fig. 3.4a). High-probability WCC hailstorms tend to form later in the day, as

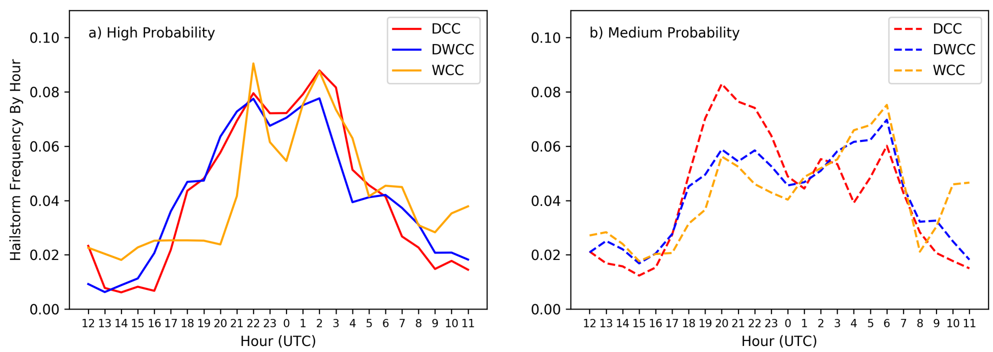

Figure 3.4: The diurnal cycle of hailstorms within the study area separated by hail probability and storm type, with panel a showing higher-probability hailstorms and panel b showing lower-probability hailstorms.

storms grow upscale, so the WCC diurnal cycle is delayed, with the maximum frequency between 22 UTC and 04 UTC. The medium-probability cases for all three types of extreme convection follow a similar diurnal pattern to their high-probability counterparts during the day and early evening through 02 UTC, although the DCCs are more favored than the other storm types during this time period (Fig. 3.4b). However, after that time, medium-probability storms have a second peak in frequency, while the high-probability cases diminish. While this was seen earlier in Figure 3.3, it is noteworthy that this overnight frequency maximum is a product of increases in the frequency of medium-probability hailstorms of all extreme storm types, but especially of WCCs and DWCCs. This overnight maximum aligns with the 06 UTC peak in heavy rainfall for this region, shown by Matsudo and Salio (2011). A picture emerges of storm severity peaking in the evening and early nighttime hours, with storm coverage and rainfall peaking later in the overnight. Consistent with this, Matsudo and Salio (2011) showed a peak in extreme wind gusts around 21 UTC, a gradual decline of wind gusts during the night, then the peak of heavy rainfall at 06 UTC.

The nocturnal maxima of hailstorms in subtropical South America can also be seen in a spatial dimension using Hovmoeller diagrams. Storms were composited for these diagrams if they occurred between 28°S and 36°S, to match the methodology of Rasmussen et al. (2014), in order to identify the unique back-building component of convection in this region. For all high-hail probability DCCs and DWCCs, storms begin to form near 18 UTC (3 pm LT) between 55°W and 65°W in response to diurnal heating (Fig. 3.5a, d). These storms then increase in frequency with time,

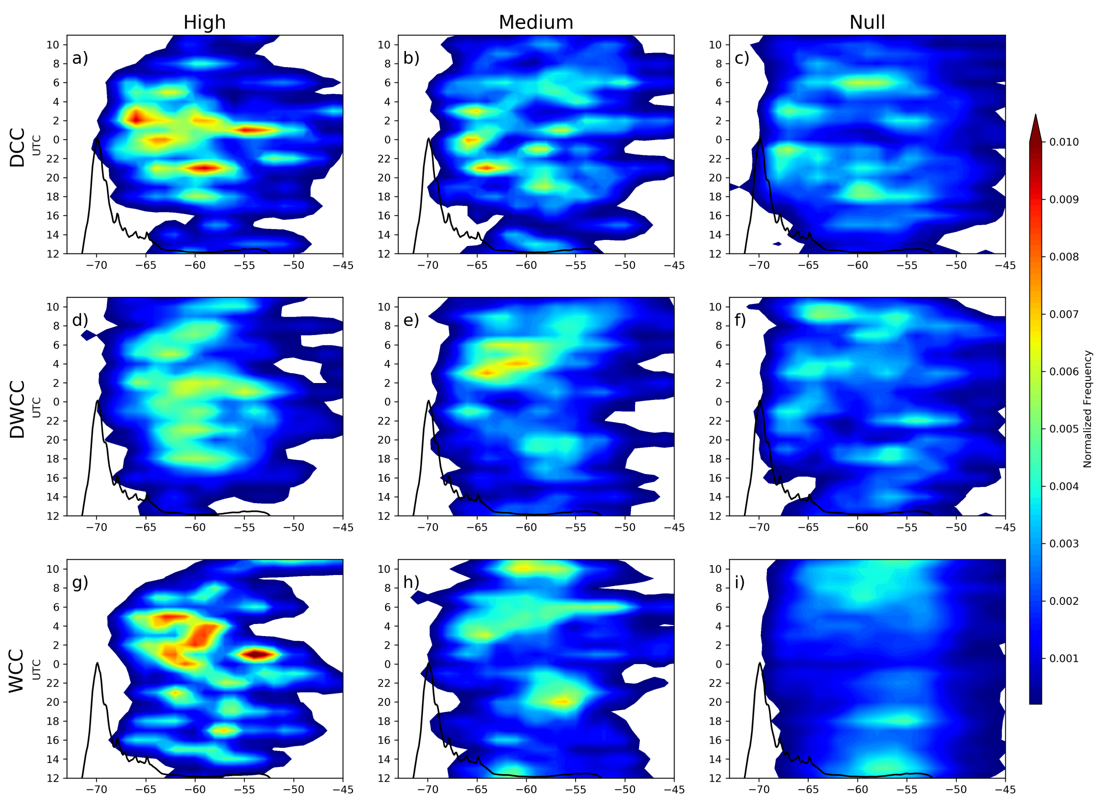

Figure 3.5: Hovmoeller diagrams of storm frequency between 28°S and 36°S, with storm type designated by row and hail probability by column. The average topography within this region is outlined in black.

but the favored locations do not move longitudinally, as was seen in similar Hovmoeller analyses of lightning flash rates within DCCs from Rasmussen et al. (2014). WCCs occur later, with maximum frequency between 00 and 06 UTC and are mostly located west of $60°$W (Fig. 3.5g). There is little eastward propagation of these storms with time, until early in the morning after 06 UTC.

For the medium-probability hailstorms, the diurnal cycle is shifted later (Fig. 3.5b, e), as shown earlier. The maximum frequency in the Hovmoeller diagrams for all three types of extreme convection occurs after 00 UTC (21 LT). Medium-probability DCCs are clearly tied to the terrain near $65°$W, and remain in place through 06 UTC. WCCs tend to propagate eastward more than the other storm types, but they also do occur over the elevated terrain for a substantial amount of time (Fig. 3.5h), which concurs with previous research in this region (Rasmussen and Houze 2011, 2016; Rasmussen et al. 2014).

The null convection cases do not seem to be specifically tied to the topography unlike the high- and medium-probability hail cases (Fig. 3.5c, f, i). There is increased frequency east of $60°$W for all null-convection storm types and reduced frequency over the mountainous areas. Therefore, if a storm contains a medium to high probability of hail, it is more likely to be located near the Andes terrain and foothills relative to storms that do not. Additionally, the locations favoring both high and medium probability hailstorms tend to remain relatively stationary near the mountains and have secondary nocturnal peaks in frequency over these areas, which has been identified by previous research as well (Rasmussen and Houze 2011; Rasmussen et al. 2014). Thus, these new results support the notion that the Andes and SDC topography is a critical ingredient in producing intense lightning- and hail-producing storms in the region.

3.3.2 Hailstorm Mode

Using the same convective storm mode definitions applied to the TRMM-based methodology as in Mulholland et al. (2018), the high-probability hailstorms that occurred between September and March were classified as discrete, multicell-organized, or multicell-unorganized. A total of 264 high-probability storms were analyzed across all storm types with the following results: 6.8%

of storms were discrete, 84.5% were multicell-organized, and 8.7% were multicell-unorganized. There is some potential bias because the ~150 km^2 TRMM 37-GHz footprint size may lead to underestimating the likelihood of hail from discrete cells, thereby preventing some discrete cells from qualifying as “high-probability” storms. With that caveat, this analysis shows that a large majority of high-probability hailstorms during the austral spring and summer are multi-cellular and that they are usually organized. This is not simply because there were more DWCC and WCC storms included in this analysis, which naturally tend to be multi-cellular, as 83% of DCCs analyzed were also multi-cellular. While this classification method is unable to diagnose rotation within storms, which affects the growth of hailstones (Ashworth and Knight 1978), these findings indicate that a majority of significant hail production does not come from discrete storms, such as supercells, but rather from organized multi-cell convection, such as MCSs.

These results stand in contrast with the hailstorms in the U.S., where a majority of hail has been found to come from discrete storms (Blair et al. 2011, 2017; Grams et al. 2011; Smith et al. 2012). Some research has shown that some multicell-organized convection can contain hail (Gallus et al. 2008), specifically organized convection that has leading-stratiform or line-parallel MCSs, but these cases are rather rare in the U.S. The satellite-based methodology used herein takes into account the hail volume in the storm and does not provide any information on the size distribution of hail within each storm. It is certainly possible that the giant hail consistently reported in subtropical South America does still occur within supercells, but is beyond the scope of the current study given observational limitations. The satellite data are also better suited for highlighting horizontally extensive storms compared to smaller ones. However, it is also likely that given the results from this analysis, MCSs in this region are more likely to produce hail relative to their counterparts in the U.S. (Rasmussen and Houze 2011). Overall, the results presented within this study suggest a significant difference in the hailstorm mode in subtropical South America that is not found in the U.S.

3.3.3 Hailstorm Characteristics

When a DCC possibly contains hail, per satellite measurements, it is likely to be horizontally larger and vertically deeper than DCCs that do not have a possibility of containing hail (Fig. 3.6). DCCs with a high probability of hail have a greater average area by more than $21,000$ km^2, while

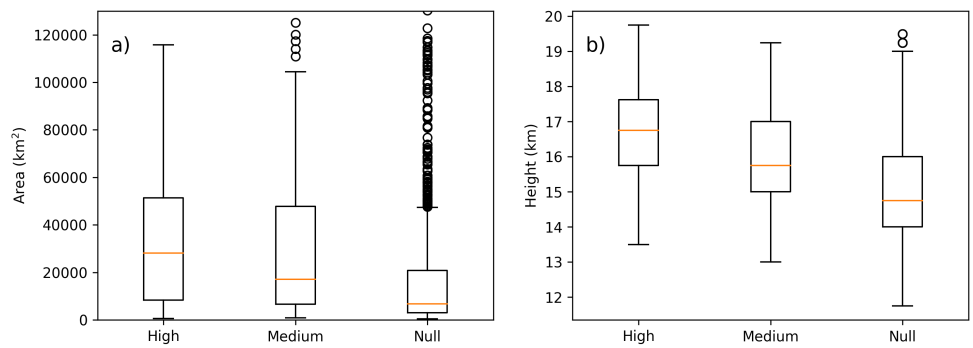

Figure 3.6: Boxplots of storm area (panel a) and maximum height (panel b) of the 40-dBZ echo core by hail threshold.

DCCs with medium hail probability have an increased area by about $16,000$ km^2. Additionally, probable DCC hailstorms tend to be deeper, by $1-2$ km on average, than DCCs without the possibility of hail. All of these differences in area and depth are significant at the 99% confidence interval. The result that deeper storms are more likely to contain hail is not a surprising one, as other recent studies using satellite-based radars have found similar results (Ni et al. 2016, 2017; Mroz et al. 2017). However, the larger horizontal area associated with hailstorms in subtropical South America is unique result to this study and supports the results from Section 3.3.2.

When a DCC has begun to grow upscale, it is likely to reach the DWCC classification, as the spatial area of its convective core increases significantly. At this stage, though, it still maintains its deep component, representing persistent and strong updrafts. For DWCCs, probable hailstorms remain larger and deeper than null convection, with the difference significant at the 99% confidence interval (Fig. 3.7). Once these storms lose their DCCs and are solely WCCs, they tend to have similar height differences between probable hailstorms and null cases, but their areas are more

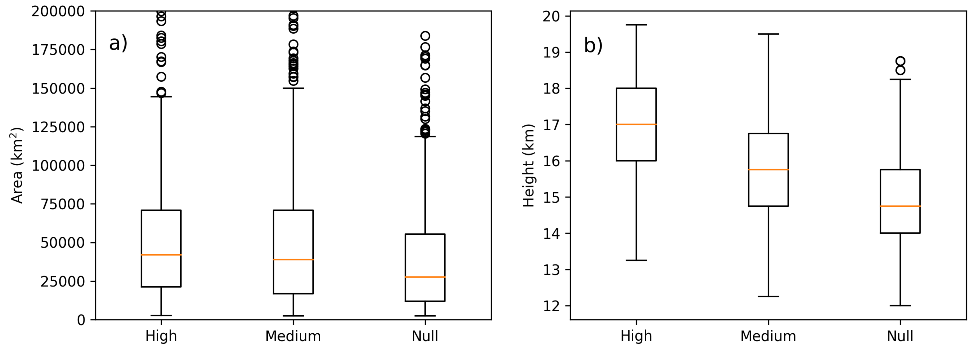

Figure 3.7: Same as Figure 3.6, but for DWCC storm area and maximum 40-dBZ echo height.

similar, as upscale growth processes mature these systems into large storms regardless of their hail production chances (Fig. 3.8).

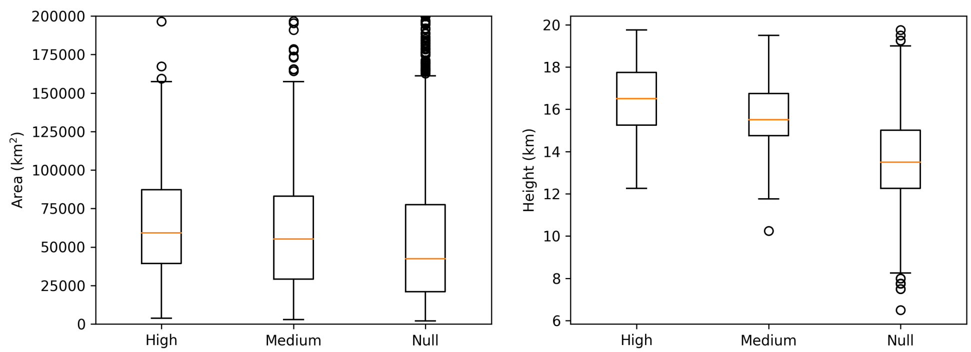

Figure 3.8: Same as Figure 3.6, but for WCC storm area and maximum 40-dBZ echo height.

In order to further understand the structure of these prolific hail-producing storms, TRMM PR reflectivity data was analyzed using Contoured Frequency by Altitude Diagrams (CFADs; Yuter and Houze 1995). At each vertical level, the frequencies are normalized by the maximum frequency at that level. For DCCs, there is a strong shift to higher reflectivities within the convective core for probable hailstorms, as compared to DCCs without the chance of hail production (Fig. 3.9a). Meanwhile, for stratiform rain, there is a shift to higher reflectivities below the melting level

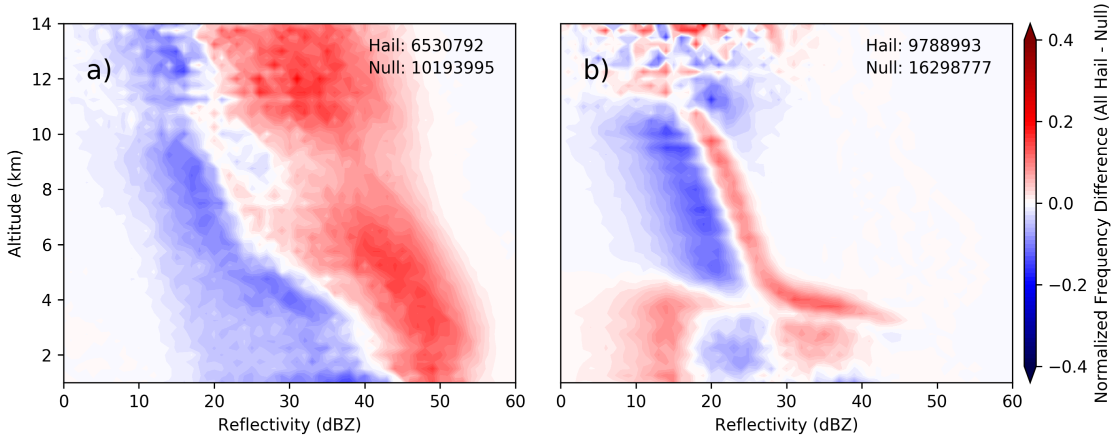

Figure 3.9: Differenced Contoured Frequency by Altitude Diagram (CFADs; Yuter and Houze 1995) for DCCs, separated by convective and stratiform rain with each vertical level normalized by the most frequent reflectivity bin within that level. Positive values represent an increase in frequency for storms with a non-zero hail probability. The number of pixels that went into each composite are listed in the top right corner of each panel.

for hailstorms (Fig. 3.9b). This increase in higher reflectivities for stratiform rain in hailstorms represents enhanced upscale growth within these storms.

Within DWCC storms, there is a greater frequency of higher reflectivities for convective rain if a storm has the possibility of containing large hail (Fig. 3.10a). Additionally, a similar signal

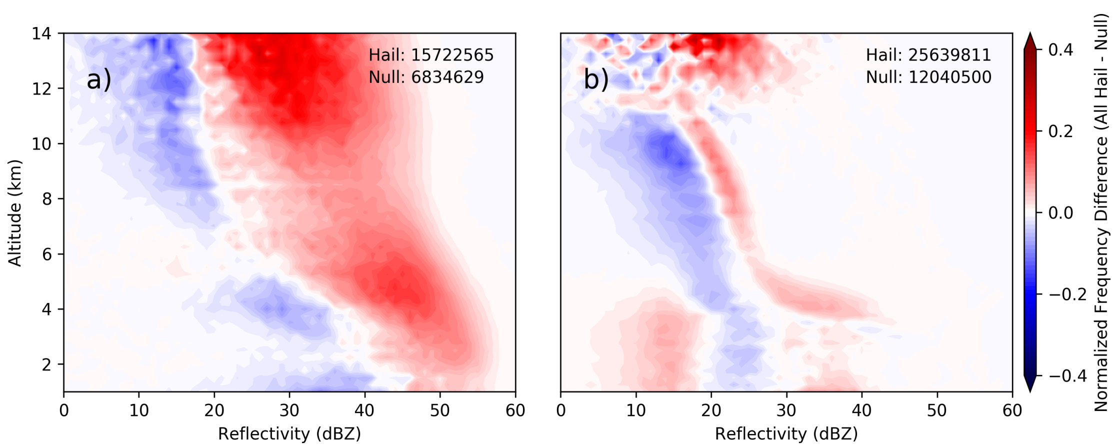

Figure 3.10: Same as Figure 3.9, but for DWCCs.

for enhanced stratiform precipitation is evident in DWCCs hailstorms as compared to DCCs hailstorms (Fig. 3.10b). However, there is also a signal for a shift to lower reflectivities for DWCC hailstorm stratiform precipitation. When these storms reach the WCC stage of their lifecycle, convective regions within hailstorms still have a strong shift to higher reflectivities than null convection (Fig. 3.11a). However, there appears to be a large amount of misclassified stratiform pixels that

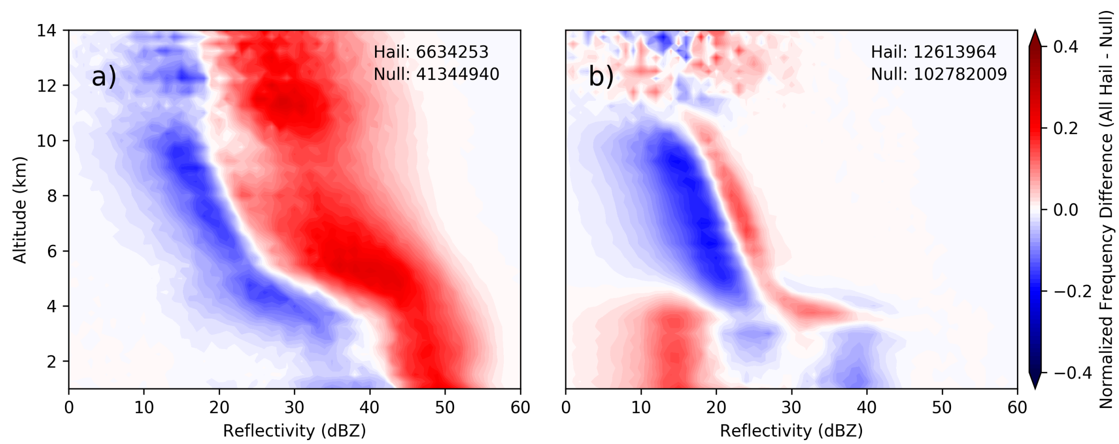

Figure 3.11: Same as Figure 3.9, but for WCCs.

are showing up in the convective profile, where the difference profile bends to higher reflectivites just below 4 km, where the melting level resides. The authors hypothesize that due to this likely misclassification, the stratiform difference CFAD is misleading by showing an increase in stratiform precipitation during WCCs that do not contain hail (Fig. 3.11b). If the rainfall was correctly classified, this would actually show the opposite result.

Overall, hailstorms are more likely to contain higher reflectivities within their convective and stratiform regions at all stages of their lifecycle than null convection. Having enhanced stratiform precipitation during the DCC and DWCC phases indicates that these storms are prone to grow upscale, even while they have vigorous deep convection, which matches the storm mode analysis discussed previously in Section 3.3.2. This is possible due to the continued lift provided by the SDC and other foothills, which promote continued convective initiation and maintenance, even while stratiform precipitation develops downstream (Rasmussen et al. 2014; Rasmussen and Houze 2011, 2016).

3.3.4 Synoptic Environments of Hailstorms

Understanding the environment that these dangerous hailstorms form in will provide better details to help forecasters warn the public in the hours and days ahead of such conditions. This analysis contains 136, 187, and 1180 unique days for high-probability hailstorms, medium-probability-hailstorms, and null storms, respectively. Examining the differences in synoptic environments between high-probability hailstorm days and null storms days, potentially useful signals for forecasting may be identified. At the surface, the lee cyclone has a central pressure 4 hPa lower during hailstorm days than during null storm days (Fig. 3.12c). This corresponds to lee cyclone development that preceded intense convection identified by Rasmussen and Houze (2016). Additionally, the 2-m temperature and dewpoint temperature increases by about $4°$C along the foothills and northern SDC (Fig. 3.12a). Meanwhile, at the 850-hPa pressure level, specific humidity is increased during hailstorm days to the east of the SDC upwards of 3 g kg^{-1} (Fig. 3.12b). The SALLJ is also strengthened, with northerly wind speeds increased by 4 m s^{-1} over northern Argentina, similar to findings from Rasmussen and Houze (2016). In the upper troposphere, a trough is moving onshore over southern South America, with ridging downstream (Fig. 3.12c, d). As a result of this anomalous height pattern, the upper-level jet stream is shifted south and the wind speed enhanced by 10 m s^{-1}. This southward shift of the jet stream places the equatorward entrance region of the jet over the SDC and foothills in central Argentina, which enables rising motion to help break any capping inversion that may exist in addition to orographic lifting.

If the same method is applied to the medium-probability hailstorm cases, similar qualitative anomalies are identified at all vertical levels (Fig. 3.13). However, the magnitude of these anomalies is reduced by approximately 50%, as the magnitude of the synoptic anomalies is correlated with the probability of hail. As a result, these synoptic anomalies for hailstorm days seem to be useful from a forecasting perspective. The low-level temperature and moisture anomalies should affect the available instability for these storms as well. Indeed, convective available potential energy (CAPE) is increased across much of the study region by an average of $600-900$ J kg^{-1} during high-probability hailstorm days and $200 - 300$ J kg^{-1} on medium-probability hailstorm days, as

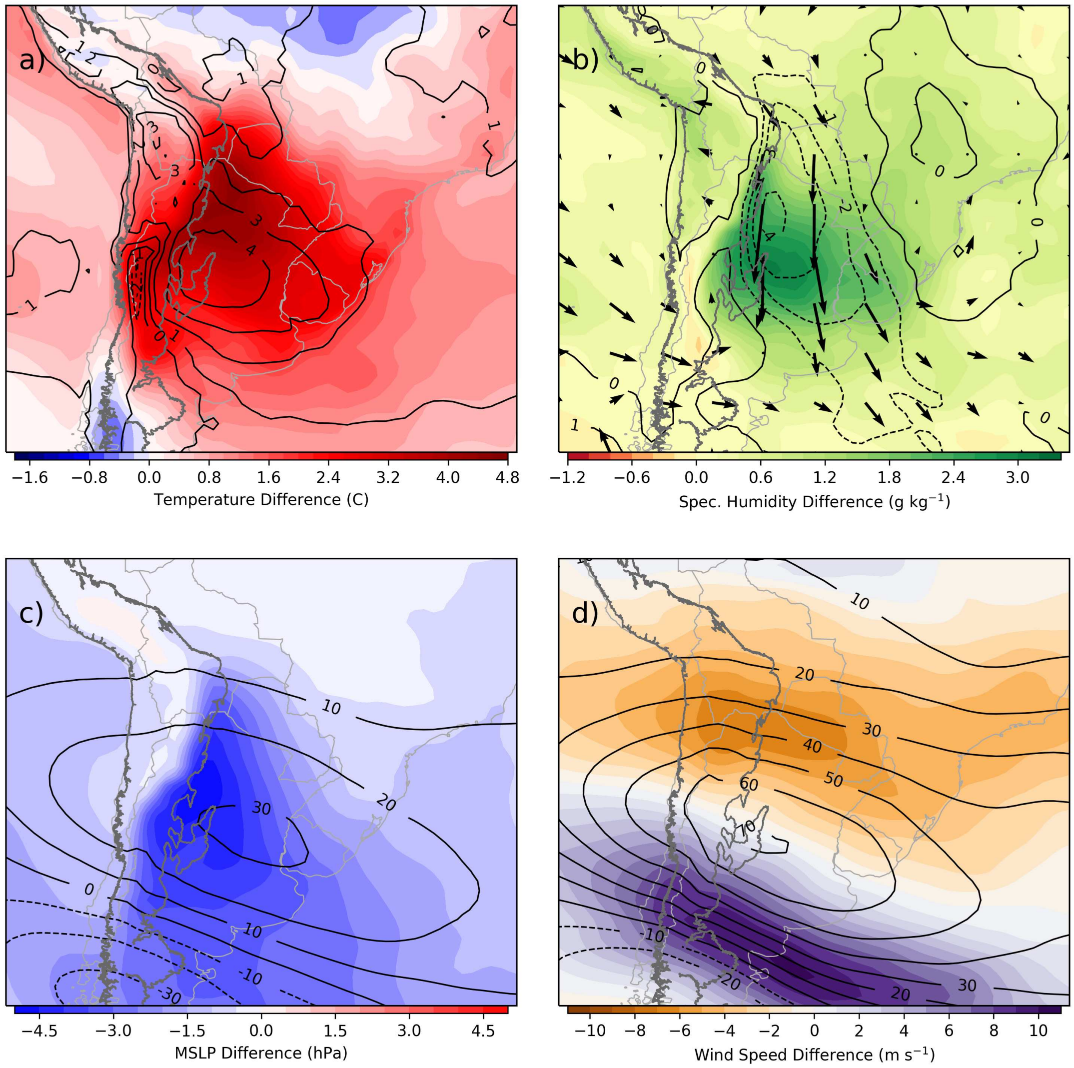

Figure 3.12: The difference between hailstorm and non-hailstorm convective days is plotted for multiple vertical levels. Convection had to occur within the primary study area in subtropical South America to be counted. Panel a displays the differences of 2-m temperature (filled) and 2-m dewpoint (contoured). Panel b shows the differences in 850-hPa specific humidity (filled) and meridional wind speed (contoured). Panel c contains the differences in mean sea-level pressure (MSLP; filled) and geopotential height (contoured). Panel d plots the differences in 250-hPa wind speed (filled) and geopotential height (contoured).

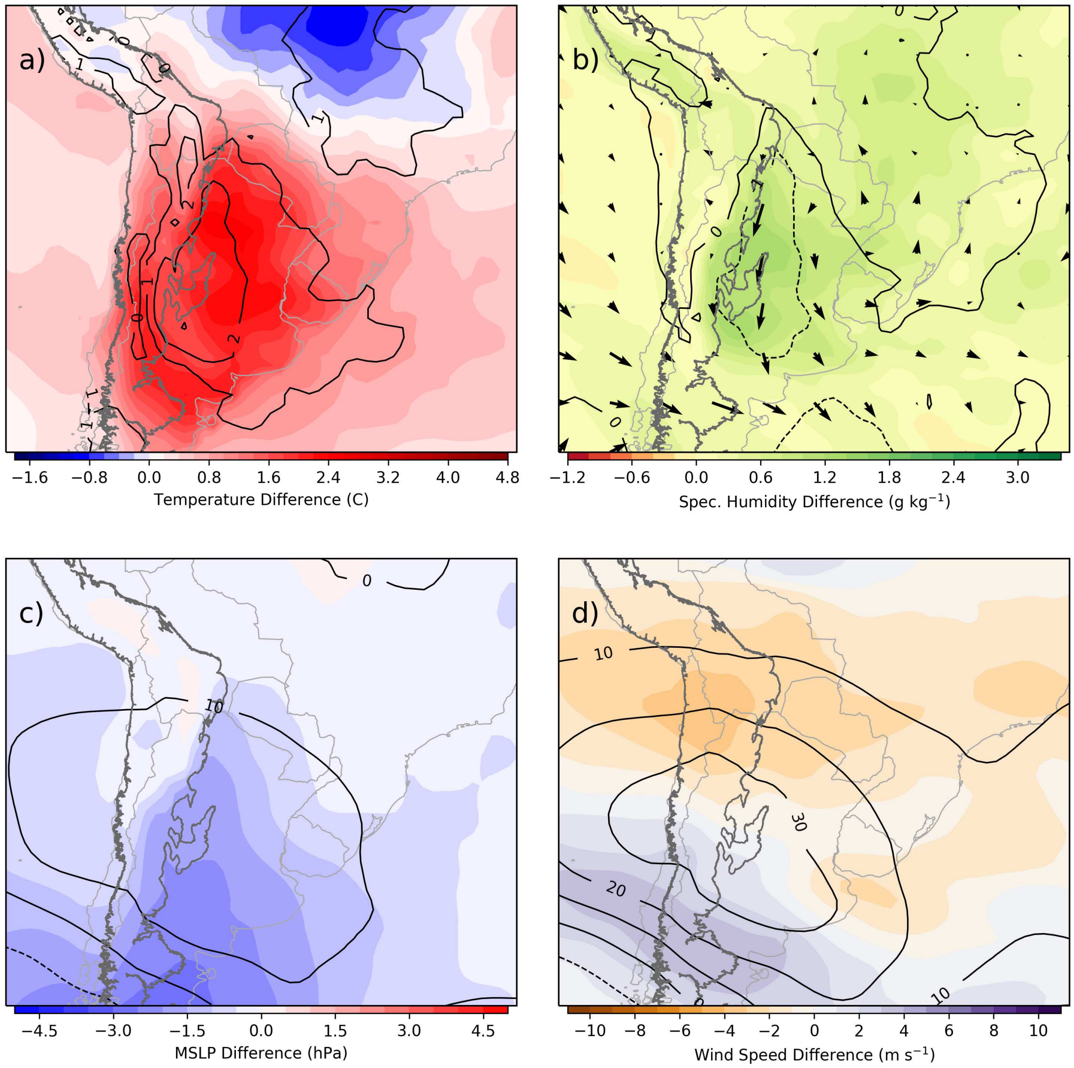

Figure 3.13: Same as Figure 3.12, but this figure shows the differences between lower-probability hail days and null convection days.

compared to null convection days (Fig. 3.14). When the maximum CAPE within the study re-

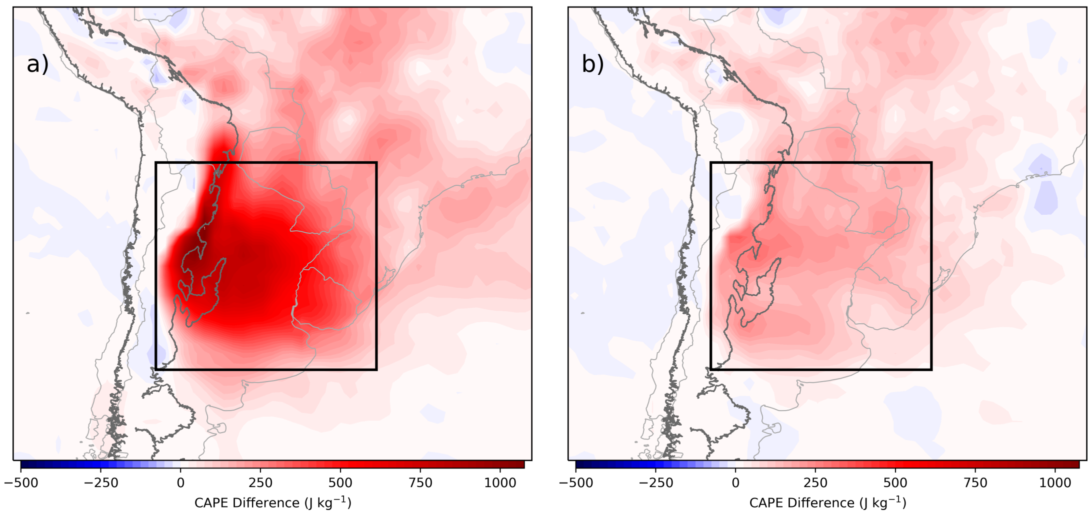

Figure 3.14: The difference between surface-based CAPE between a) upper-threshold hail days and null convection days and b) lower-threshold hail days and null convection days.

gion is compared between the hail probability and null categories, there is also a clear distinction between days that contained storms with much likelihood of hail as compared to days with null storm cases, even though they still contained convection (Fig. 3.15). The mean maximum CAPE values for high-probability, medium-probability, and null hailstorm days are 3439, 2835, and 2416 J kg^{-1}, respectively. The difference between these means is statistically significant at the 99% confidence interval. By enhancing instability, stronger updrafts are able to form, which would be more capable of supporting large hail.

Overall, these hailstorms appear to be more strongly forced by the synoptic environment compared to the null convection category. This may be a product of the requirements to form hail: steep lapse rates, low freezing levels, and strong vertical wind shear. All of these ingredients are more easily produced by strong synoptic forcing, such as when a trough is moving into the region, bringing colder upper-level air and a strong jet stream. Through these enhanced synoptic conditions, hailstorms can more easily form in this region, often with very large hail. These results

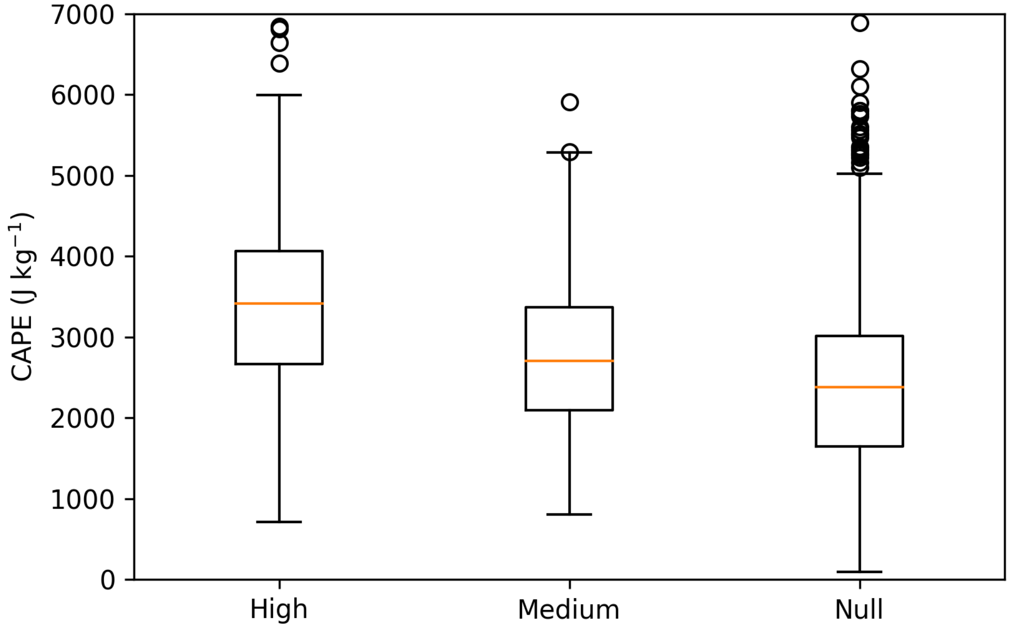

Figure 3.15: Boxplot of the maximum CAPE found within the study region based upon the maximum hail probability found within the region on a particular day.

do not preclude hailstorm formation within weakly forced environments, but rather they show the tendency to have these strong storms occur in strongly-forced synoptic conditions.

3.4 Conclusion

Convection in subtropical South America is known to be some of the most intense anywhere on Earth. As a result, understanding the severe convective hazards produced by storms within this region is critical, as they threaten personal safety, agriculture, and socioeconomic considerations in Argentina. Within this region, hail is notably large and frequent in occurrence compared to other regions of the world, but little work has been done to understand hailstorm characteristics, structure, or supporting environments. This study aims to provide insight into this important problem by utilizing long-term satellite measurements of intense convection to identify hailstorm characteristics and their supporting environments to provide a greater understanding of high-impact weather around the world.

Hailstorms are found to have an expected annual cycle, with the maximum hailstorm activity occurring during the spring and summer. However, hailstorms in subtropical South America have an extended diurnal cycle, compared to that found in the U.S., with a substantial portion of the distribution occurring during the overnight period. Additionally, a large majority (84%) of these storms were found to be organized multi-cellular convection. Both the diurnal cycle and storm mode of hailstorms in subtropical South America are notably different from hailstorms in the U.S. that are primarily discrete storms that occur in the late afternoon hours. Hailstorms in this region also tend to be deeper and larger in horizontal area than storms that do not contain hail. Finally, hailstorms are supported by enhanced synoptic conditions, including increased instability through low-level temperature and moisture increases, an enhanced lee trough and SALLJ, and stronger upper-level jet streams.

Hailstorms in subtropical South America are some of the most frequent and intense in the world. While they are supported synoptically by similar conditions to those found in the U.S., the storm mode and diurnal cycles of these storms are very different. As a result, they prove to be a challenge to forecast from numerical and operational perspectives, as the knowledge gained by studying U.S. hailstorms does not apply to this region as well as might be expected. Therefore, the results of the RELAMPAGO field campaign will be critical in improving the understanding of hailstorms within this region. Additionally, new understandings about hailstorm characteristics and associated environmental conditions in subtropical South America may aid the comprehension of hailstorms in the U.S. and other regions of the world, which in turn will improve forecasting of these dangerous storms. Future work will make use of the observations from this campaign to better understand why the diurnal cycle of hailstorms extends into the overnight hours, in addition to the analysis of rotation within storms and its role in supporting hailstone growth in a variety of convective modes.

Chapter 4

Conclusion

Convection produces severe hazardous weather worldwide, impacting people and property through high winds, large hail, flash floods, and tornadoes. While these dangerous thunderstorms can occur throughout many regions of the world, they are most frequent near major mountain ranges, such as the Andes, Rocky, and Himalayan mountains. Understanding the variability and characteristics of convection is critically important in order to improve the prediction of such storms and increase the resiliency of affected populations. Additionally, the knowledge gained by studying the distribution of convective variability in subtropical South America, from inter-storm to interannual scales, can be applied to other similar regions of the world for enhanced global understanding of convective variability and associated storm characteristics.

This thesis presents two studies on convection in subtropical South America, specifically examining how ENSO affects the extreme convective distribution and discovering the characteristics of hailstorms in this region. Convection in subtropical South America is among the strongest anywhere in the world. Through these studies, short- and long-term forecasts of hazardous convective weather can be improved through a greater understanding of how the climate variability affects convection and how and when hail-producing convection is forced by synoptic conditions and orography. As a result, better preparations can be made for seasonal and interannual rainfall variations and convective changes due to ENSO, along with improved employment of hail mitigation techniques with the enhanced understanding of when, where, and why hailstorms form and produce extremely large hail. Climatologically, more rain falls over the La Plata basin during El Nino, while the Amazon receives more rainfall during La Nina. Synoptically, the lower- and upper-level jets are enhanced during El Nino, with a stronger lee trough at the surface. With regards to ENSO's influence on convection within subtropical South America, DCCs tend to be more common during El Niño near the high terrain, while wide convective cores are more common throughout subtropical South America during La Niña. However, during El Niño, storms tend to be deeper and contain stronger convection. They are also supported by enhanced synoptic conditions, including a stronger upper-level jet stream and increased instability. However, these results do not mean that there is any significant decrease in severe hazards presented by these storms.

Hailstorms tend to be some of the deepest and widest convection found within this region. They have a much longer diurnal cycle than hailstorms in other regions of the world, with a relative nocturnal maximum in frequency. Finally, hailstorms are supported by strongly-forced synoptic environments and the tall mountains nearby, which promote strong convective initiation, upscale growth, and back-building over time. Without the orographic lift provided by the Andean foothills and Sierras de Cordoba, the strong mechanical capping inversion would not be broken as frequently and these hailstorms would occur significantly less often. As a result of their concentrated frequency, longevity, and power, these storms present a significant threat to society and the agricultural economy.

With the results presented in this thesis, decision-makers can better prepare for hazardous convective weather on short and long timescales to improve resiliency to these natural hazards. Additionally, the results of the recent RELAMPAGO field campaign will be placed in the context of this work and previous studies of convection within subtropical South America. With time, ground-based observations of storms can be compared with satellite-based studies to provide a more holistic depiction of the strong and frequent convection here. Furthermore, it will promote better understanding of convection around the world, especially where it occurs near other significant mountain ranges, such as the Himalayas, central and southern Africa, and the U.S. TRMM satellite observations, which these findings are based upon, have proved quite useful in examining convection in under-sampled regions such as subtropical South America, and this work further promotes the utility of these space-based platforms. With the addition of the Global Precipitation Measurement satellite in recent years, this method of research will continue to provide meaningful results for regions around the world where ground-based observations remain limited.

Bibliography

Allen, J. T., and M. K. Tippett, 2015: The Characteristics of United States Hail Reports: 1955-2014. *E-Journal of Severe Storms Meteorology*, **10 (3)**, URL http://www.ejssm.org/ojs/index.php/ejssm/article/view/149.

Allen, J. T., M. K. Tippett, and A. H. Sobel, 2015: Influence of the El Niño/Southern Oscillation on tornado and hail frequency in the United States. *Nature Geoscience*, **8 (4)**, 278–283, doi:10.1038/ngeo2385, URL https://www.nature.com/articles/ngeo2385.

Anderson, C. J., and R. W. Arritt, 2001: Mesoscale Convective Systems over the United States during the 1997–98 El Niño. *Monthly Weather Review*, **129 (9)**, 2443–2457, doi:10.1175/1520-0493(2001)129<2443:MCSOTU>2.0.CO;2, URL https://journals.ametsoc.org/doi/abs/10.1175/1520-0493(2001)129%3C2443:MCSOTU%3E2.0.CO%3B2.

Arkin, P. A., 1982: The Relationship Between Interannual Variability in the 200 mb Tropical Wind Field and the Southern Oscillation. *Monthly Weather Review*, **110 (10)**, 1393–1404, doi:10.1175/1520-0493(1982)110<1393:TRBIVI>2.0.CO;2, URL https://journals.ametsoc.org/doi/abs/10.1175/1520-0493%281982%29110%3C1393%3ATRBIVI%3E2.0.CO%3B2.

Ashworth, T., and C. A. Knight, 1978: Cylindrical Ice Accretions as Simulations of Hail Growth: I. Effects of Rotation and of Mixed Clouds. *Journal of the Atmospheric Sciences*, **35 (10)**, 1987–1996, doi:10.1175/1520-0469(1978)035<1987:CIAASO>2.0.CO;2, URL https://journals.ametsoc.org/doi/abs/10.1175/1520-0469(1978)035%3C1987:CIAASO%3E2.0.CO%3B2.

Awaka, J., T. Iguchi, H. Kumagai, and K. Okamoto, 1997: Rain type classification algorithm for TRMM precipitation radar. *Geoscience and Remote Sensing, 1997. IGARSS '97. Remote Sensing - A Scientific Vision for Sustainable Development., 1997 IEEE International*, Vol. 4, 1633–1635 vol.4, doi:10.1109/IGARSS.1997.608993.

Bjerknes, J., 1969: Atmospheric teleconnections from the equatorial pacific. *Monthly Weather Review*, **97 (3)**, 163–172, doi:10.1175/1520-0493(1969)097<0163:ATFTEP>2.3.CO;2, URL https://journals.ametsoc.org/doi/abs/10.1175/1520-0493%281969%29097%3C0163%3AATFTEP%3E2.3.CO%3B2.

Blair, S. F., D. R. Deroche, J. M. Boustead, J. W. Leighton, B. L. Barjenbruch, and W. P. Gargan, 2011: A Radar-Based Assessment of the Detectability of Giant Hail. *E-Journal of Severe Storms Meteorology*, **6 (7)**, URL http://www.ejssm.org/ojs/index.php/ejssm/article/view/87.

Blair, S. F., and Coauthors, 2017: High-Resolution Hail Observations: Implications for NWS Warning Operations. *Weather and Forecasting*, **32 (3)**, 1101–1119, doi:10.1175/WAF-D-16-0203.1, URL https://journals.ametsoc.org/doi/full/10.1175/WAF-D-16-0203.1.

Blamey, R. C., C. Middleton, C. Lennard, and C. J. C. Reason, 2017: A climatology of potential severe convective environments across South Africa. *Climate Dynamics*, **49 (5-6)**, 2161–2178, doi:10.1007/s00382-016-3434-7, URL https://link.springer.com/article/10.1007/s00382-016-3434-7.

Camilloni, I. A., and V. R. Barros, 2003: Extreme discharge events in the Parana River and their climate forcing. *Journal of Hydrology*, **278**, 94–106, doi:https://doi.org/10.1016/S0022-1694(03)00133-1, URL https://www.sciencedirect.com/science/article/pii/S0022169403001331.

Cavalcanti, I., and Coauthors, 2015: Precipitation extremes over La Plata Basin - Review and new results from observations and climate simulations. *Journal of Hydrology*, **523**, 211–230, doi:https://doi.org/10.1016/j.jhydrol.2015.01.028, URL https://www.sciencedirect.com/science/article/pii/S0022169415000451.

Cecil, D. J., 2009: Passive Microwave Brightness Temperatures as Proxies for Hailstorms. *Journal of Applied Meteorology and Climatology*, **48 (6)**, 1281–1286, doi:10.1175/2009JAMC2125.1, URL https://journals.ametsoc.org/doi/abs/10.1175/2009JAMC2125.1.

Cecil, D. J., and C. B. Blankenship, 2012: Toward a Global Climatology of Severe Hailstorms as Estimated by Satellite Passive Microwave Imagers. *Journal of Climate*, **25 (2)**, 687–703, doi:10.1175/JCLI-D-11-00130.1, URL https://journals.ametsoc.org/doi/abs/10.1175/JCLI-D-11-00130.1.

Cecil, D. J., and T. Chronis, 2018: Polarization Corrected Temperatures for 10-, 19-, 37-, and 89-GHz Passive Microwave Frequencies. *Journal of Applied Meteorology and Climatology*, doi:10.1175/JAMC-D-18-0022.1, URL https://journals.ametsoc.org/doi/abs/10.1175/JAMC-D-18-0022.1.

Chronis, T. G., S. J. Goodman, D. Cecil, D. Buechler, F. J. Robertson, J. Pittman, and R. J. Blakeslee, 2008: Global lightning activity from the ENSO perspective. *Geophysical Research Letters*, **35 (19)**, doi:10.1029/2008GL034321, URL https://agupubs.onlinelibrary.wiley.com/doi/full/10.1029/2008GL034321.

Cintineo, J. L., T. M. Smith, V. Lakshmanan, H. E. Brooks, and K. L. Ortega, 2012: An Objective High-Resolution Hail Climatology of the Contiguous United States. *Weather and Forecasting*, **27 (5)**, 1235–1248, doi:10.1175/WAF-D-11-00151.1, URL https://journals.ametsoc.org/doi/full/10.1175/WAF-D-11-00151.1.

Cook, A. R., L. M. Leslie, D. B. Parsons, and J. T. Schaefer, 2017: The Impact of El Niño–Southern Oscillation (ENSO) on Winter and Early Spring U.S. Tornado Outbreaks. *Journal of Applied Meteorology and Climatology*, **56 (9)**, 2455–2478, doi:10.1175/JAMC-D-16-0249.1, URL https://journals.ametsoc.org/doi/full/10.1175/JAMC-D-16-0249.1.

Cook, A. R., and J. T. Schaefer, 2008: The Relation of El Niño–Southern Oscillation (ENSO) to Winter Tornado Outbreaks. *Monthly Weather Review*, **136 (8)**, 3121–3137, doi:10.1175/2007MWR2171.1, URL https://journals.ametsoc.org/doi/abs/10.1175/2007MWR2171.1.

Dai, A., 2001: Global Precipitation and Thunderstorm Frequencies. Part I: Seasonal and Interannual Variations. *Journal of Climate*, **14 (6)**, 1092–1111, doi:10.1175/1520-0442(2001)

014<1092:GPATFP>2.0.CO;2, URL https://journals.ametsoc.org/doi/full/10.1175/1520-0442\%282001\%29014\%3C1092\%3AGPATFP\%3E2.0.CO\%3B2.

Dee, D. P., and Coauthors, 2011: The ERA-Interim reanalysis: configuration and performance of the data assimilation system. *Quarterly Journal of the Royal Meteorological Society*, **137 (656)**, 553–597, doi:10.1002/qj.828, URL http://onlinelibrary.wiley.com/doi/10.1002/qj.828/abstract.

Durkee, J. D., T. L. Mote, and J. M. Shepherd, 2009: The Contribution of Mesoscale Convective Complexes to Rainfall across Subtropical South America. *Journal of Climate*, **22 (17)**, 4590–4605, doi:10.1175/2009JCLI2858.1, URL https://journals.ametsoc.org/doi/abs/10.1175/2009JCLI2858.1.

Espinoza Villar, J. C., and Coauthors, 2009: Spatio-temporal rainfall variability in the Amazon basin countries (Brazil, Peru, Bolivia, Colombia, and Ecuador). *International Journal of Climatology*, **29 (11)**, 1574–1594, doi:10.1002/joc.1791, URL http://onlinelibrary.wiley.com/doi/10.1002/joc.1791/abstract.

Etkin, D., and S. E. Brun, 2001: *Canada's Hail Climatology [electronic Resource] : 1977-1993*. Institute for Catastrophic Loss Reduction, URL http://0361572.netsolhost.com/images/Canada_s_Hail_Climatology.pdf, google-Books-ID: Kl6gtgEACAAJ.

Frisby, E. M., and H. W. Sansom, 1967: Hail Incidence in the Tropics. *Journal of Applied Meteorology*, **6 (2)**, 339–354, doi:10.1175/1520-0450(1967)006<0339:HIITT>2.0.CO;2, URL https://journals.ametsoc.org/doi/10.1175/1520-0450%281967%29006%3C0339%3AHIITT%3E2.0.CO%3B2.

Gallus, W. A., N. A. Snook, and E. V. Johnson, 2008: Spring and Summer Severe Weather Reports over the Midwest as a Function of Convective Mode: A Preliminary Study. *Weather and Forecasting*, **23 (1)**, 101–113, doi:10.1175/2007WAF2006120.1, URL https://journals.ametsoc.org/doi/full/10.1175/2007WAF2006120.1.

Gonzalez, M. H., E. M. Garbarini, A. L. Rolla, and S. Eslamian, 2017: Meteorological Drought Indices: Rainfall Prediction in Argentina. *Handbook of Drought and Water Scarcity, Vol. 1: Principles of Drought and Water Scarcity*, Vol. 1, Francis and Taylor, USA, 541–570.

Grams, J. S., R. L. Thompson, D. V. Snively, J. A. Prentice, G. M. Hodges, and L. J. Reames, 2011: A Climatology and Comparison of Parameters for Significant Tornado Events in the United States. *Weather and Forecasting*, **27 (1)**, 106–123, doi:10.1175/WAF-D-11-00008.1, URL https://journals.ametsoc.org/doi/full/10.1175/WAF-D-11-00008.1.

Grandoso, H. N., and J. V. Iribarne, 1963: Evaluation of the first three years in a hail prevention experiment in mendoza (Argentina). *Zeitschrift für angewandte Mathematik und Physik ZAMP*, **14 (5)**, 549–553, doi:10.1007/BF01601262, URL https://doi.org/10.1007/BF01601262.

Grimm, A. M., and T. Ambrizzi, 2009: Teleconnections into South America from the Tropics and Extratropics on Interannual and Intraseasonal Timescales. *Past Climate Variability in South America and Surrounding Regions: From the Last Glacial Maximum to the Holocene*, F. Vimeux, F. Sylvestre, and M. Khodri, Eds., Developments in Paleoenvironmental Research, Springer Netherlands, Dordrecht, 159–191, doi:10.1007/978-90-481-2672-9_7, URL https://doi.org/10.1007/978-90-481-2672-9_7.

Grimm, A. M., V. R. Barros, and M. E. Doyle, 2000: Climate Variability in Southern South America Associated with El Niño and La Niña Events. *Journal of Climate*, **13 (1)**, 35–58, doi:10.1175/1520-0442(2000)013<0035:CVISSA>2.0.CO;2, URL https://journals.ametsoc.org/doi/full/10.1175/1520-0442%282000%29013%3C0035%3ACVISSA%3E2.0.CO%3B2.

Grimm, A. M., and R. G. Tedeschi, 2009: ENSO and Extreme Rainfall Events in South America. *Journal of Climate*, **22 (7)**, 1589–1609, doi:10.1175/2008JCLI2429.1, URL https://journals.ametsoc.org/doi/full/10.1175/2008JCLI2429.1.

Halpert, M. S., and C. F. Ropelewski, 1992: Surface Temperature Patterns Associated with the Southern Oscillation. *Journal of Climate*, **5 (6)**, 577–593, doi:10.1175/

1520-0442(1992)005<0577:STPAWT>2.0.CO;2, URL https://journals.ametsoc.org/doi/abs/10.1175/1520-0442%281992%29005%3C0577%3ASTPAWT%3E2.0.CO%3B2.

Hendon, H. H., 2003: Indonesian Rainfall Variability: Impacts of ENSO and Local Air–Sea Interaction. *Journal of Climate*, **16 (11)**, 1775–1790, doi:10.1175/1520-0442(2003)016<1775:IRVIOE>2.0.CO;2, URL https://journals.ametsoc.org/doi/full/10.1175/1520-0442%282003%29016%3C1775%3AIRVIOE%3E2.0.CO%3B2.

Horel, J. D., and J. M. Wallace, 1981: Planetary-Scale Atmospheric Phenomena Associated with the Southern Oscillation. *Monthly Weather Review*, **109 (4)**, 813–829, doi:10.1175/1520-0493(1981)109<0813:PSAPAW>2.0.CO;2, URL https://journals.ametsoc.org/doi/abs/10.1175/1520-0493%281981%29109%3C0813%3APSAPAW%3E2.0.CO%3B2.

Houze, R. A., 2004: Mesoscale convective systems. *Reviews of Geophysics*, **42 (4)**, RG4003, doi:10.1029/2004RG000150, URL http://onlinelibrary.wiley.com/doi/10.1029/2004RG000150/abstract.

Houze, R. A., K. L. Rasmussen, M. D. Zuluaga, and S. R. Brodzik, 2015: The variable nature of convection in the tropics and subtropics: A legacy of 16 years of the Tropical Rainfall Measuring Mission satellite. *Reviews of Geophysics*, **53 (3)**, 994–1021, doi:10.1002/2015RG000488, URL http://onlinelibrary.wiley.com/doi/10.1002/2015RG000488/full.

Houze, R. A., D. C. Wilton, and B. F. Smull, 2007: Monsoon convection in the Himalayan region as seen by the TRMM Precipitation Radar. *Quarterly Journal of the Royal Meteorological Society*, **133 (627)**, 1389–1411, doi:10.1002/qj.106, URL http://onlinelibrary.wiley.com/doi/10.1002/qj.106/abstract.

Huffman, G. J., and Coauthors, 2007: The TRMM Multisatellite Precipitation Analysis (TMPA): Quasi-Global, Multiyear, Combined-Sensor Precipitation Estimates at Fine Scales. *Journal of Hydrometeorology*, **8 (1)**, 38–55, doi:10.1175/JHM560.1, URL https://journals.ametsoc.org/doi/abs/10.1175/JHM560.1.

Iguchi, T., T. Kozu, J. Kwiatkowski, R. Meneghini, J. Awaka, and K. Okamoto, 2009: Uncertainties in the Rain Profiling Algorithm for the TRMM Precipitation Radar. *Journal of the Meteorological Society of Japan*, **87A**, 1–30, doi:https://doi.org/10.2151/jmsj.87A.1, URL https://www.jstage.jst.go.jp/article/jmsj/87A/0/87A_0_1/_article.

Iguchi, T., T. Kozu, R. Meneghini, J. Awaka, and K. Okamoto, 2000: Rain-Profiling Algorithm for the TRMM Precipitation Radar. *Journal of Applied Meteorology*, **39 (12)**, 2038–2052, doi:10.1175/1520-0450(2001)040<2038:RPAFTT>2.0.CO;2, URL https://journals.ametsoc.org/doi/abs/10.1175/1520-0450(2001)040%3C2038%3ARPAFTT%3E2.0.CO%3B2.

Karoly, D. J., 1989: Southern Hemisphere Circulation Features Associated with El Niño-Southern Oscillation Events. *Journal of Climate*, **2 (11)**, 1239–1252, doi:10.1175/1520-0442(1989)002<1239:SHCFAW>2.0.CO;2, URL https://journals.ametsoc.org/doi/abs/10.1175/1520-0442(1989)002\%3C1239:SHCFAW\%3E2.0.CO\%3B2.

Karyampudi, V. M., M. L. Kaplan, S. E. Koch, and R. J. Zamora, 1995: The Influence of the Rocky Mountain on the 13–14 April 1986 Severe Weather Outbreak. Part I: Mesoscale Lee Cyclogenesis and Its Relationship to Severe Weather and Dust Storms. *Monthly Weather Review*, **123 (5)**, 1394–1422, doi:10.1175/1520-0493(1995)123<1394:TIOTRM>2.0.CO;2, URL https://journals.ametsoc.org/doi/abs/10.1175/1520-0493(1995)123\%3C1394\%3ATIOTRM\%3E2.0.CO\%3B2.

Kousky, V. E., M. T. Kagano, and I. F. A. Cavalcanti, 1984: A review of the Southern Oscillation: oceanic-atmospheric circulation changes and related rainfall anomalies. *Tellus A*, **36A (5)**, 490–504, doi:10.1111/j.1600-0870.1984.tb00264.x, URL https://onlinelibrary.wiley.com/doi/abs/10.1111/j.1600-0870.1984.tb00264.x.

Kummerow, C., W. Barnes, T. Kozu, J. Shiue, and J. Simpson, 1998: The Tropical Rainfall Measuring Mission (TRMM) Sensor Package. *Journal of Atmospheric and Oceanic Technology*, **15 (3)**, 809–817, doi:10.1175/1520-0426(1998)015<0809:TTRMMT>2.0.CO;2, URL https://journals.ametsoc.org/doi/abs/10.1175/1520-0426(1998)015%3C0809%3ATTRMMT%3E2.0.CO%3B2.

Kummerow, C., and Coauthors, 2000: The Status of the Tropical Rainfall Measuring Mission (TRMM) after Two Years in Orbit. *Journal of Applied Meteorology*, **39 (12)**, 1965–1982, doi:10.1175/1520-0450(2001)040<1965:TSOTTR>2.0.CO;2, URL https://journals.ametsoc.org/doi/abs/10.1175/1520-0450(2001)040%3C1965:TSOTTR%3E2.0.CO;2.

Lee, S.-K., B. E. Mapes, C. Wang, D. B. Enfield, and S. J. Weaver, 2014: Springtime ENSO phase evolution and its relation to rainfall in the continental U.S. *Geophysical Research Letters*, **41 (5)**, 2013GL059 137, doi:10.1002/2013GL059137, URL http://onlinelibrary.wiley.com/doi/10.1002/2013GL059137/abstract.

Lichtenstein, E. R., 1980: La depresión del Noroeste argentino. Text, Facultad de Ciencias Exactas y Naturales. Universidad de Buenos Aires, URL https://digital.bl.fcen.uba.ar/gsdl-282/cgi-bin/library.cgi?a=d&c=tesis&d=Tesis_1649_Lichtenstein.

Liebmann, B., and J. A. Marengo, 2001: Interannual Variability of the Rainy Season and Rainfall in the Brazilian Amazon Basin. *Journal of Climate*, **14 (22)**, 4308–4318, URL http://www.jstor.org/stable/26249079.

Makitov, V., 1999: Organization and Main Results of the Hail Suppression Program in the Northern Area of the Province of Mendoza, Argentina. *The Journal of Weather Modification*, **31 (1)**, 76–86, URL http://journalofweathermodification.org/index.php/JWM/article/view/250.

Matsudo, C. M., and P. V. Salio, 2011: Severe weather reports and proximity to deep convection over Northern Argentina. *Atmospheric Research*, **100 (4)**, 523–537, doi:10.1016/j.atmosres.2010.11.004, URL http://www.sciencedirect.com/science/article/pii/S0169809510003078.

Mezher, R. N., M. Doyle, and V. Barros, 2012: Climatology of hail in Argentina. *Atmospheric Research*, **114-115**, 70–82, doi:10.1016/j.atmosres.2012.05.020, URL http://www.sciencedirect.com/science/article/pii/S0169809512001597.

Mroz, K., A. Battaglia, T. J. Lang, D. J. Cecil, S. Tanelli, and F. Tridon, 2017: Hail-Detection Algorithm for the GPM Core Observatory Satellite Sensors. *Journal of Applied Meteorology* *and Climatology*, **56 (7)**, 1939–1957, doi:10.1175/JAMC-D-16-0368.1, URL https://journals.ametsoc.org/doi/full/10.1175/JAMC-D-16-0368.1.

Mulholland, J. P., S. W. Nesbitt, R. J. Trapp, K. L. Rasmussen, and P. V. Salio, 2018: Convective Storm Life Cycle and Environments near the Sierras de Córdoba, Argentina. *Monthly Weather Review*, **146 (8)**, 2541–2557, doi:10.1175/MWR-D-18-0081.1, URL https://journals.ametsoc.org/doi/abs/10.1175/MWR-D-18-0081.1.

Ni, X., C. Liu, D. J. Cecil, and Q. Zhang, 2017: On the Detection of Hail Using Satellite Passive Microwave Radiometers and Precipitation Radar. *Journal of Applied Meteorology and Climatology*, **56 (10)**, 2693–2709, doi:10.1175/JAMC-D-17-0065.1, URL https://journals.ametsoc.org/doi/10.1175/JAMC-D-17-0065.1.

Ni, X., C. Liu, Q. Zhang, and D. J. Cecil, 2016: Properties of hail storms over China and the United States from the Tropical Rainfall Measuring Mission. *Journal of Geophysical Research: Atmospheres*, **121 (20)**, 12,031–12,044, doi:10.1002/2016JD025600, URL https://agupubs.onlinelibrary.wiley.com/doi/abs/10.1002/2016JD025600.

Parhi, P., A. Giannini, P. Gentine, and U. Lall, 2015: Resolving Contrasting Regional Rainfall Responses to El Niño over Tropical Africa. *Journal of Climate*, **29 (4)**, 1461–1476, doi:10.1175/JCLI-D-15-0071.1, URL https://journals.ametsoc.org/doi/full/10.1175/JCLI-D-15-0071.1.

Perez, R. C., and E. Puliafito, 2006: Study of hailstorms cells producing big damages in Mendoza (Argentina). *Proceedings of ERAD*, 4, URL http://www.crahi.upc.edu/ERAD2006/proceedingsMask/00136.pdf.

Pocakal, D., Z. Večenaj, and J. Stalec, 2009: Hail characteristics of different regions in continental part of Croatia based on influence of orography. *Atmospheric Research*, **93 (1)**, 516–525, doi:10.1016/j.atmosres.2008.10.017, URL http://www.sciencedirect.com/science/article/pii/S0169809508003049.

Prieto, R., L. Gimeno, R. García, R. Herrera, E. Hernández, and P. Ribera, 1999: Interannual variability of hail-days in the Andes region since 1885. *Earth and Planetary Science Letters*, **171 (3)**, 503–509, doi:10.1016/S0012-821X(99)00170-3, URL http://www.sciencedirect.com/science/article/pii/S0012821X99001703.

Qie, X., X. Wu, T. Yuan, J. Bian, and D. Lu, 2014: Comprehensive Pattern of Deep Convective Systems over the Tibetan Plateau–South Asian Monsoon Region Based on TRMM Data. *Journal of Climate*, **27 (17)**, 6612–6626, doi:10.1175/JCLI-D-14-00076.1, URL https://journals.ametsoc.org/doi/full/10.1175/JCLI-D-14-00076.1.

Rasmussen, K. L., M. M. Chaplin, M. D. Zuluaga, and R. A. Houze, 2016: Contribution of Extreme Convective Storms to Rainfall in South America. *Journal of Hydrometeorology*, **17 (1)**, 353–367, doi:10.1175/JHM-D-15-0067.1, URL https://journals.ametsoc.org/doi/abs/10.1175/JHM-D-15-0067.1.

Rasmussen, K. L., S. L. Choi, M. D. Zuluaga, and R. A. Houze, 2013: TRMM precipitation bias in extreme storms in South America. *Geophysical Research Letters*, **40 (13)**, 3457–3461, doi:10.1002/grl.50651, URL http://onlinelibrary.wiley.com/doi/10.1002/grl.50651/abstract.

Rasmussen, K. L., and R. A. Houze, 2011: Orogenic Convection in Subtropical South America as Seen by the TRMM Satellite. *Monthly Weather Review*, **139 (8)**, 2399–2420, doi:10.1175/MWR-D-10-05006.1, URL http://journals.ametsoc.org/doi/abs/10.1175/MWR-D-10-05006.1.

Rasmussen, K. L., and R. A. Houze, 2016: Convective Initiation near the Andes in Subtropical South America. *Monthly Weather Review*, **144 (6)**, 2351–2374, doi:10.1175/MWR-D-15-0058.1, URL https://journals.ametsoc.org/doi/abs/10.1175/MWR-D-15-0058.1.

Rasmussen, K. L., M. D. Zuluaga, and R. A. Houze, 2014: Severe convection and lightning in subtropical South America. *Geophysical Research Letters*, **41 (20)**, 2014GL061 767, doi:10.1002/2014GL061767, URL http://onlinelibrary.wiley.com/doi/10.1002/2014GL061767/abstract.

Rasmusson, E. M., and T. H. Carpenter, 1983: The Relationship Between Eastern Equatorial Pacific Sea Surface Temperatures and Rainfall over India and Sri Lanka. *Monthly Weather Review*, **111 (3)**, 517–528, doi:10.1175/1520-0493(1983)111<0517:TRBEEP>2.0.CO;2, URL https://journals.ametsoc.org/doi/10.1175/1520-0493%281983%29111%3C0517%3ATRBEEP%3E2.0.CO%3B2.

Rayner, N. A., D. E. Parker, E. B. Horton, C. K. Folland, L. V. Alexander, D. P. Rowell, E. C. Kent, and A. Kaplan, 2003: Global analyses of sea surface temperature, sea ice, and night marine air temperature since the late nineteenth century. *Journal of Geophysical Research: Atmospheres*, **108 (D14)**, 4407, doi:10.1029/2002JD002670, URL http://onlinelibrary.wiley.com/doi/10.1029/2002JD002670/abstract.

Romatschke, U., and R. A. Houze, 2010: Extreme Summer Convection in South America. *Journal of Climate*, **23 (14)**, 3761–3791, doi:10.1175/2010JCLI3465.1, URL https://journals.ametsoc.org/doi/abs/10.1175/2010JCLI3465.1.

Romatschke, U., and R. A. Houze, 2011: Characteristics of Precipitating Convective Systems in the South Asian Monsoon. *Journal of Hydrometeorology*, **12 (1)**, 3–26, doi:10.1175/2010JHM1289.1, URL https://journals.ametsoc.org/doi/abs/10.1175/2010JHM1289.1.

Romatschke, U., S. Medina, and R. A. Houze, 2010: Regional, Seasonal, and Diurnal Variations of Extreme Convection in the South Asian Region. *Journal of Climate*, **23 (2)**, 419–439, doi:10.1175/2009JCLI3140.1, URL https://journals.ametsoc.org/doi/full/10.1175/2009JCLI3140.1.

Ropelewski, C. F., and M. S. Halpert, 1987: Global and Regional Scale Precipitation Patterns Associated with the El Niño/Southern Oscillation. *Monthly Weather Review*, **115 (8)**, 1606–1626, doi:10.1175/1520-0493(1987)115<1606:GARSPP>2.0.CO;2, URL https://journals.ametsoc.org/doi/10.1175/1520-0493%281987%29115%3C1606%3AGARSPP%3E2.0.CO%3B2.

Roy, S. S., S. B. Saha, S. K. R. Bhowmik, and P. K. Kundu, 2014: Optimization of Nowcast Software WDSS-II for operational application over the Indian region. *Meteorology and Atmospheric*

Physics, **124 (3-4)**, 143–166, doi:10.1007/s00703-014-0315-7, URL https://link.springer.com/article/10.1007/s00703-014-0315-7.

Sanchez, J. L., and Coauthors, 2009: Characterization of hailstone size spectra in hailpad networks in France, Spain, and Argentina. *Atmospheric Research*, **93 (1)**, 641–654, doi:10.1016/j.atmosres.2008.09.033, URL http://www.sciencedirect.com/science/article/pii/S0169809508002615.

Seluchi, M. E., A. C. Saulo, M. Nicolini, and P. Satyamurty, 2003: The Northwestern Argentinean Low: A Study of Two Typical Events. *Monthly Weather Review*, **131 (10)**, 2361–2378, doi:10.1175/1520-0493(2003)131<2361:TNALAS>2.0.CO;2, URL https://journals.ametsoc.org/doi/10.1175/1520-0493%282003%29131%3C2361%3ATNALAS%3E2.0.CO%3B2.

Shimizu, M. H., T. Ambrizzi, and B. Liebmann, 2017: Extreme precipitation events and their relationship with ENSO and MJO phases over northern South America. *International Journal of Climatology*, **37**, doi:10.1002/joc.4893, URL http://onlinelibrary.wiley.com/doi/10.1002/joc.4893/epdf.

Smith, B. T., R. L. Thompson, J. S. Grams, C. Broyles, and H. E. Brooks, 2012: Convective Modes for Significant Severe Thunderstorms in the Contiguous United States. Part I: Storm Classification and Climatology. *Weather and Forecasting*, **27 (5)**, 1114–1135, doi:10.1175/WAF-D-11-00115.1, URL https://journals.ametsoc.org/doi/full/10.1175/WAF-D-11-00115.1.

Smith, S. B., and M. K. Yau, 1993: The Causes of Severe Convective Outbreaks in Alberta. Part II: Conceptual Model and Statistical Analysis. *Monthly Weather Review*, **121 (4)**, 1126–1133, doi:10.1175/1520-0493(1993)121<1126:TCOSCO>2.0.CO;2, URL https://journals.ametsoc.org/doi/10.1175/1520-0493%281993%29121%3C1126%3ATCOSCO%3E2.0.CO%3B2.

Souza, E. B. D., and T. Ambrizzi, 2002: ENSO impacts on the South American rainfall during 1980s: Hadley and Walker circulation. *Atmósfera*, **15 (2)**, 105–120, URL http://www.scielo.org.mx/scielo.php?script=sci_abstract&pid=S0187-62362002000200003&lng=es&nrm=iso&tlng=en.

Sulca Juan, Takahashi Ken, Espinoza Jhan-Carlo, Vuille Mathias, and Lavado-Casimiro Waldo, 2017: Impacts of different ENSO flavors and tropical Pacific convection variability (ITCZ, SPCZ) on austral summer rainfall in South America, with a focus on Peru. *International Journal of Climatology*, **38 (1)**, 420–435, doi:10.1002/joc.5185, URL https://rmets.onlinelibrary.wiley.com/doi/full/10.1002/joc.5185.

Tippett, M. K., J. T. Allen, V. A. Gensini, and H. E. Brooks, 2015: Climate and Hazardous Convective Weather. *Current Climate Change Reports*, **1 (2)**, 60–73, doi:10.1007/s40641-015-0006-6, URL https://link.springer.com/article/10.1007/s40641-015-0006-6.

Trenberth, K. E., 1997: The Definition of El Niño. *Bulletin of the American Meteorological Society*, **78 (12)**, 2771–2778, doi:10.1175/1520-0477(1997)078<2771:TDOENO>2.0.CO;2, URL https://journals.ametsoc.org/doi/abs/10.1175/1520-0477(1997)078%3C2771:TDOENO%3E2.0.CO;2.

Velasco, I., and J. M. Fritsch, 1987: Mesoscale convective complexes in the Americas. *Journal of Geophysical Research: Atmospheres*, **92 (D8)**, 9591–9613, doi:10.1029/JD092iD08p09591, URL http://onlinelibrary.wiley.com/doi/10.1029/JD092iD08p09591/abstract.

Wallace, J. M., and D. S. Gutzler, 1981: Teleconnections in the Geopotential Height Field during the Northern Hemisphere Winter. *Monthly Weather Review*, **109 (4)**, 784–812, doi:10.1175/1520-0493(1981)109<0784:TITGHF>2.0.CO;2, URL https://journals.ametsoc.org/doi/10.1175/1520-0493%281981%29109%3C0784%3ATITGHF%3E2.0.CO%3B2.

Williams, L., 1973: *Hail and Its Distribution: Report No. 8 of "Studies of the Army Aviation V/STOL Environment"*. Engineer Topographic Laboratories, google-Books-ID: ifIikgAACAAJ.

Yoshida, S., T. Morimoto, T. Ushio, and Z. Kawasaki, 2007: ENSO and convective activities in Southeast Asia and western Pacific. *Geophysical Research Letters*, **34 (21)**, doi:10.1029/2007GL030758, URL https://agupubs.onlinelibrary.wiley.com/doi/full/10.1029/2007GL030758.

Yuter, S. E., and R. A. Houze, 1995: Three-Dimensional Kinematic and Microphysical Evolution of Florida Cumulonimbus. Part II: Frequency Distributions of Vertical Velocity, Reflectivity, and Differential Reflectivity. *Monthly Weather Review*, **123 (7)**, 1941–1963, doi:10.1175/1520-0493(1995)123<1941:TDKAME>2.0.CO;2, URL https://journals.ametsoc.org/doi/abs/10.1175/1520-0493(1995)123%3C1941%3ATDKAME%3E2.0.CO%3B2.

Zhang, C., Q. Zhang, and Y. Wang, 2008: Climatology of Hail in China: 1961–2005. *Journal of Applied Meteorology and Climatology*, **47 (3)**, 795–804, doi:10.1175/2007JAMC1603.1, URL https://journals.ametsoc.org/doi/full/10.1175/2007JAMC1603.1.

Zipser, E. J., D. J. Cecil, C. Liu, S. W. Nesbitt, and D. P. Yorty, 2006: Where are the most intense thunderstorms on earth? *Bulletin of the American Meteorological Society*, **87 (8)**, 1057–1072, doi:10.1175/BAMS-87-8-1057, URL https://journals.ametsoc.org/doi/abs/10.1175/BAMS-87-8-1057.

Zuluaga, M. D., and R. A. Houze, 2015: Extreme Convection of the Near-Equatorial Americas, Africa, and Adjoining Oceans as seen by TRMM. *Monthly Weather Review*, **143 (1)**, 298–316, doi:10.1175/MWR-D-14-00109.1, URL https://journals.ametsoc.org/doi/abs/10.1175/MWR-D-14-00109.1.